The variability and predictability of the IRI shape parameters over Grahamstown, South Africa

A thesis submitted in partial fulfillment of the
requirements for the degree of

Master of Science

of

RHODES UNIVERSITY

by

Oyapo Chimidza

September 2007

Contents

Abstract

The International Reference Ionosphere (IRI) shape parameters B_0, B_1, and D_1 provide a representation of the shape of the F_2 layer, the thickness of the F_2 layer and the shape of the F_1 layer of the ionosphere respectively. The aim of this study was to examine the variability of these parameters using Grahamstown, South Africa (33.3°S, 26.5°E) ionosonde data and determine their predictability by the IRI-2001 model. A further aim of this study was to investigate developing an alternative model for predicting these parameters. These parameters can be determined from electron density profiles that are inverted from ionograms recorded with an ionosonde. Data representing the B_0, B_1 and D_1 parameters, with half hourly or hourly intervals, were scaled and deduced from the digital pulse sounder (DPS) ionosonde for the period April 1996 to December 2006. An analysis of the diurnal, seasonal, and solar variations of the behaviour of these parameters was undertaken for the years 2000, 2004 and 2005 using monthly medians. Comparisons between the observational results and that of the IRI model (IRI 2001 version) indicate that the IRI-2001 model does not accurately represent the diurnal and seasonal variation of the parameters. A preliminary model was thus developed using the technique of Neural Networks (NNs). All available data from the Grahamstown ionosonde from 1996 to 2006 were used in the training of the NNs and the prediction of the variation of the shape parameters. Inputs to the model were the day number, the hour of day, the solar activity and the magnetic index. Comparisons between the preliminary NN model and the IRI-2001 model indicated that the preliminary model was more accurate at the prediction of the parameters than the IRI-2001 model. This analysis showed the need to improve the existing IRI model or develop a new model for the South African region. This thesis describes the results from this feasibility study which show the variability and predictability of the IRI shape parameters.

Acknowledgements

I would like to convey special thanks to my supervisors Dr Lee-Anne McKinnell and Dr P. J. Cilliers for the invaluable support and help they gave me in conducting this research. Special thanks to John Bosco Habarulema, Zama Katamzi and Patrick Sibanda who are fellow students for the timeless help they gave me in times of need. May the Lord be with them.

I thank Hermanus Magnetic Observatory and the department of Physics and Electronics at Rhodes University for availing their equipment and data to enable me to conduct the research to its completion. Finaly I thank NASSP for having given me a place in their programme which enabled me to get into this research area.

Chapter 1

Introduction

The aim of this research is to investigate the variability of the IRI shape parameters, B_0, B_1 and D_1, applicable to Grahamstown (33.3°S, 26.5°E), South Africa. An additional aim of this research is to model the IRI shape parameters.

This research represents a first effort to study the variability of the IRI shape parameters, B_0, B_1 and D_1 with season and solar cycle and the ability of the IRI model to predict them for the South African region. This study will help in establishing the suitability of the IRI (2001 version) model for predicting the shape parameters over this part of the globe. If possible, the results from this study could be incorporated into the IRI model in order to improve it. Deficiencies in the model to date, have been reported to the IRI working group and this study could be of use to the IRI community [Bilitza *et al*, 2000].

1.1 The IRI

The IRI model is established by a joint working group of the Committee on Space Research (COSPAR) and the International Union of Radio Science (URSI). The IRI describes monthly averages of the electron density, electron temperature, ion temperature and ion composition in the altitude range of about 50 km to 1000 km for magnetically quiet conditions in the non-auroral ionosphere [Bilitza, 1990]. The IRI model has been significantly improved by means of ground and space data collected throughout the world. The research and studies that have led to several IRI updates are presented and discussed at annual IRI workshops and then published in the journal *Advances in Space Research*.

In the early 1960's COSPAR decided that a set of empirically based tables describing the

upper atmosphere should be established. The first findings were presented in 1961. In the subsequent years more data from a number of theoretical approaches was collected and this resulted in the release of improved models. This undertaking proved to be a success and it led to the establishment of a comparable reference for the ionized constituents of the atmosphere called the International Reference Ionosphere (IRI). The IRI was to contain empirically based tables describing monthly median vertical profiles of the main parameters of the ionospheric plasma. This was to be used as a standard reference for the design of experiments, the estimation of the atmospheric environment and other effects, and for checking theories, among others. The profiles were to be provided for suitably chosen locations, hours, seasons and levels of solar activity [Bilitza, 1990].

Since the inception of the IRI it has been found that the electron density profile database contains numerous gaps and does not provide uniform worldwide coverage. In spite of this, the working group has come up with the IRI tables method for the prediction of the global electron density. True height profiles of electron density and plasma composition were only available for a small number of stations providing, by no means, a global coverage. The inversion technique, needed to obtain true height profiles, had been applied only at very few places at temperate latitudes. The full (vertical) profile of the plasma density was described by a set of mathematical expressions, each valid in a certain height range. This complex system allowed a correct representation of the most important inputs, like the peak densities of the main layers [Bilitza, 1990].

The first IRI was released in 1978 and it was critically tested with a wide variety of data. Since 1982 COSPAR together with URSI have organised yearly workshop meetings to discuss and improve the model. The computer code used by the IRI model has been changed step by step and new features introduced as they become available. The existing database was insufficient to provide a full representation and as a result special data analysis and collection efforts were undertaken in different countries [Bilitza, 1990]. Rawer *et al*, (1978) noted a few open problems, among them a need for an improved database in the low latitude belt. Also pointed out, was the need for improving the thickness and shape parameters, B_0 and B_1 of the F_2 layer, and the shape parameter, D_1 of the F_1 layer provided by the IRI [Bilitza, 1990] to model the bottomside electron density profile. This was pointed out by the IRI Task Force Activity (TFA's) that took place at the Aeronomy and Radio Propagation Laboratory of the International Center of Theoretical Physics (ICTP), in Trieste, Italy between 19 and 23 August 1996.

Recently Bilitza *et al*, (2000) carried out a study using data from several stations that had not yet been used in the IRI development, and deduced a new table for B_0 values that

was included in the new version of IRI [Olazábal *et al*, 2004]. Reinisch and Huang (2000) provided a new formulation for the presentation of the F_1 layer in the IRI electron density profile that avoids the difficulties found in IRI-90 for the modeling of the F_1 profile. In view of all these; there is a need to undertake these kinds of studies in geographical areas where data has not been available for incorporation into the IRI and to determine the local variability of the IRI profile parameters in such areas. More details on the definitions of the IRI shape parameters will be provided in chapter 2.

The IRI model is a global empirical model for the non-auroral, quiet ionosphere. A variety of analytical expressions and functions are used in the IRI to represent temporal and spatial variations in the ionospheric densities and temperatures. Global variations (with latitude and longitude/local time) are in most cases described by a form of spherical harmonics series (Legrendre polynomials) [Bilitza, 1990]. Over the years testing and modification of the IRI has continued with extensive participation by the international research community and it has led to improvements through several versions (IRI-80, IRI-86, IRI-90, IRI-95, etc) [Sethi and Pandey, 2001]. The model provides a basis for the simulation and prediction of the ionospheric radio wave propagation.

Epstein functions have been used in the IRI to represent altitudinal, latitudinal and diurnal features. The first three members of the Epstein family of functions are [Bilitza, 1990]

$$EPS_{-1}(h; HX, SC) = ln(1 + e^x) \tag{1.1}$$

$$EPS_0(h; HX, SC) = \frac{1}{(1 + e^{-x})} \tag{1.2}$$

$$EPS_1(h; HX, SC) = \frac{e^x}{(1 + e^x)^2} \tag{1.3}$$

with

$$x = \frac{(h - HX)}{SC} \tag{1.4}$$

and

$$EPS_{i+1} = \frac{d(EPS_i)}{dx} \tag{1.5}$$

EPS_{-1} describes a transition, EPS_0 a step and EPS_1 a peak at $h = HX$ with the width SC. The Epstein functions are shown in figure 1.1 [Bilitza, 1990]. There are three filter functions which can be used for a joint analytical representation of the whole electron density profile. These are explained in Rawer (1987) and will not be dealt with here.

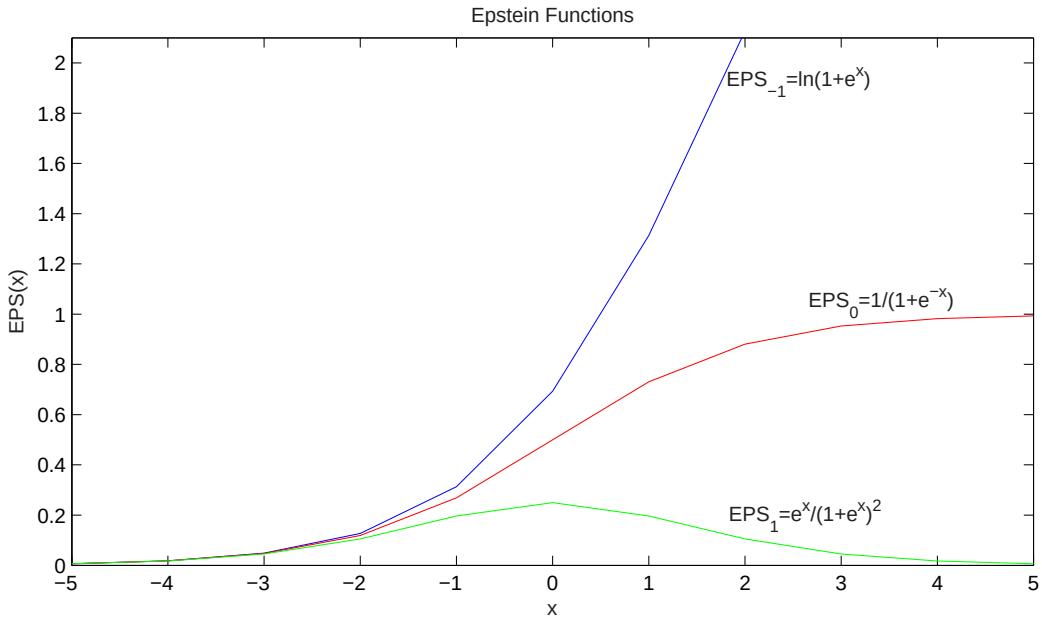

Figure 1.1: Epstein Functions

1.2 The ionosphere

The ionosphere is the part of the earth's atmosphere that is sufficiently ionized by solar Extreme Ultra-Violet (EUV) and Ultra-Violet (UV) radiation. This region does not have specific boundaries, but covers the altitude range from about 50 km to 1000 km. The behaviour of the ionosphere is complex because of the processes acting on and within the region. The ionosphere is multi-layered and these layers can be divided into three different regions namely: (1) lower ionosphere (between about 50 km to 90 km); (2) bottomside ionosphere (between about 90 km and 350 km); and (3) the topside ionosphere (above about 350 km). The bottomside ionosphere is further divided into the E and F layers. The F region is subdivided into two regions called the F_1 and the F_2 layers. The F_2 layer is usually where the maximum electron density occurs. These layers are defined by the dominant ions that are present at different altitudes. The structure of the ionosphere is not constant but varies with variations in the solar radiation and the Earth's magnetic field [Langley, 2000].

The radiation from the sun ionizes constituent particles in the ionosphere, which in turn affects the propagation of radio waves. The electron density distribution in the Earth's ionosphere displays a marked variation with altitude, latitude, longitude , universal time, season, solar cycle, and magnetic activity. The variation is primarily a result of the ionosphere's coupling with other regions in the solar terrestrial system, including the sun and the interplanetary medium. The ionosphere's absorption of the radiation increases with decreasing altitude and the density of molecules and neutral atoms. This results in the formation of

maximum electron density layers. The main source of plasma and energy for the ionosphere is solar EUV and UV radiation, but magnetospheric electric fields and particle precipitation have a significant effect on the system. The ionization is greater during daytime as compared to nighttime due to the influx of the solar radiation from the sun. This results in having only a diminished F_2 layer present at nighttime due to the absence of the solar radiation in the atmosphere. Ionization is also greater during sunspot cycle peaks due to increased solar activity. The degree of ionization and the height of the ionized layers fluctuate diurnally, seasonally and with geographic location.

The ionospheric variations are also influenced by the strong coupling processes to regions below and above it. Below the ionosphere there is a dense neutral atmosphere, which is modulated by the tropospheric weather and surface topology. Above the ionosphere there are space plasma processes in the magnetosphere, caused by its coupling to the interplanetary magnetic field and the solar wind. This interface provides highly variable inputs of energetic particles and electrodynamic energy. These can cause the ionospheric variations to be very complex. The variations can be long term down to operational time-scales of days, hours or even minutes [Rishbeth and Mendillo, 2001]. There are many references to ionospheric variations and the ability to model such complex variations, but the reader is referred to Davies, 1990 for a simple mathematical view of these variations.

The distribution of electrons thins out with altitude, which makes the upper boundary of the ionosphere not well defined. Because of the complicated nature of the ionosphere, there have been numerous approaches to ionospheric modeling over the years. These approaches include: (1) Empirical models based on extensive worldwide data sets; (2) Three-dimensional time dependent physical models including self-consistent coupling to other solar terrestrial regions; (3) Analytical models based on orthogonal function fit to the output obtained from numerical models; and (4) Models driven by real-time ionospheric inputs [Kohl et al, 1996].

1.3 Thesis outline

The theoretical background for the bottomside ionosphere including the formulae for the diffrerent layers and profiles will be discussed in chapter 2. Chapter 3 will deal with the handling of the data, making the profiles and the comparisons of the graphs to the IRI model. The development of the Neural Network (NN) based model is discussed in chapter 4, where results are compared with those from the IRI model.

Chapter 2

Background

2.1 Introduction

This chapter presents a detailed background theory of the bottomside ionosphere together with the formulae describing the shape of the bottomside profile.

2.2 The IRI shape parameters

2.2.1 Electron density

Different layers in the ionosphere are shown in figure 2.1. Each layer has its own characteristic critical frequency. The IRI electron densities are normalised to the F peak in the upper ionosphere and to the E peak in the lower ionosphere and these two parts are merged in the E valley region [Bilitza, 2000]. Different layers in the ionosphere have boundaries which have characteristic profile points. The critical frequencies are f_oF_2 for the F_2 layer, f_oF_1 for the F_1 layer and f_oE for the E layer. A radio wave with a critical frequency f_oF_2 transmitted vertically from the ground will be reflected at the F_2-peak [Bilitza, 1990]. The relationship between the electron density, N_mF and the critical frequency, f at a height where the wave is reflected is given by

$$N_mF = 1.24 * 10^{10} * f^2 \tag{2.1}$$

where N_mF is the peak density of the particular F layer given in units of m^-3 and f is the frequency in MHz.

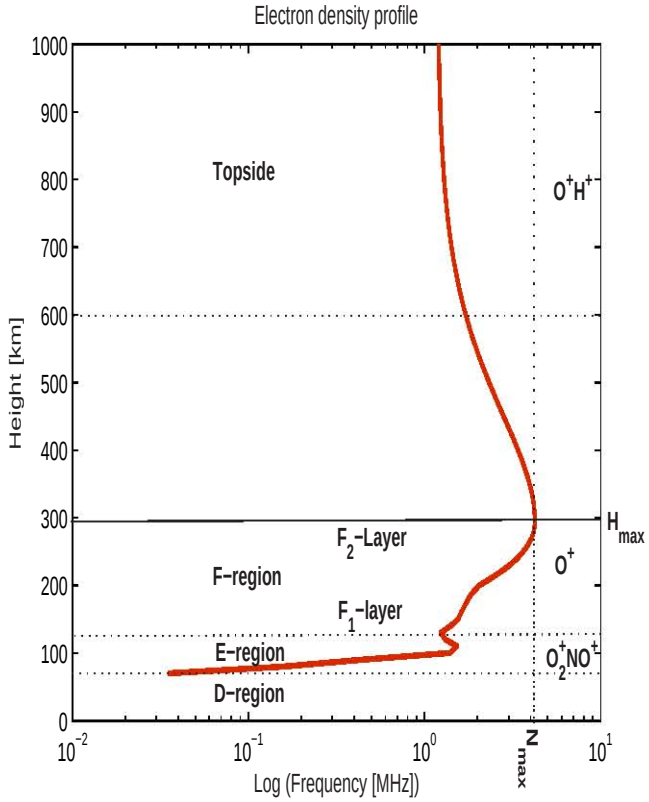

Figure 2.1: Electron Density profile showing different layers

2.2.2 Bottomside (h_mF_1 to h_mF_2)

The IRI model for the bottomside F_2 layer electron density profile uses an analytic formula which is described in terms of four parameters: the F_2 peak density, N_mF_2, the F_2 peak height, h_mF_2, the bottomside thickness parameter, B_0 and the shape parameter, B_1; [Bilitza, 1990]

$$\frac{N(h)}{N_mF_2} = \frac{e^{-X^{B_1}}}{cosh(X)} \tag{2.2}$$

where

$$X = \frac{(h_mF_2 - h)}{B_0} \tag{2.3}$$

Equation 2.3 is only valid for h less than h_mF_2. The bottomside thickness parameter, B_0 is the height difference between h_mF_2 and the height $h_{0.24}$. The height $h_{0.24}$ is the point where the electron density profile has dropped to 0.24 of the maximum electron density of the F_2 layer, (N_mF_2). The B_1 parameter determines the shape of the profile between the heights h_mF_2 and $h_{0.24}$. It is clear from the above equations that the entire profile is specified

by only two parameters, B_0 and B_1. This is a simple approach as long as equation (2.2) precisely represents the vertical electron density distribution in the F_2 region. A plot of X versus the normalised electron density (figure 2.2) shows the behaviour of the IRI profile for different values of B_1. The values of the electron density N and the corresponding plasma frequency f_N at $X = 1$ are $N = N_1 = 0.24N_mF_2$ and $f = f_1 = 0.49f_0F_2$ independent of B_1 as shown by figure 2.2. At $X = 1$ equation (2.3) gives $h = h_mF_2 - B_0$, hence B_0 is the height difference between h_mF_2 and $h = h(N_1) = h_{0.24}$. B_1 controls the profile shape in this height interval as evidenced from the different plots of B_1 in figure 2.2 [Reinisch and Huang, 1998]. The larger the values of B_1 the larger the densities in that region [Bilitza *et al*, 2000]. The current IRI bottomside electron density model is based on the work of Ramakrishnan and Rawer (1972). They established $B_1 = 3$ as the best choice and compiled a table for B_0 values based on $B_1 = 3$ for different seasons, local times and latitude ranges [Radicella *et al*, 1998]. In IRI B_1 is set to 3 and then increased in increments of 0.5 if merging between the F_2 bottomside profile and the E-valley profile cannot be accomplished. These increments facilitate the merging of the E and F regions. When merging becomes difficult to get this could lead to discontinuities or artificial valleys [Bilitza, 2001]. Reinish and Huang (2000) have developed a better functional description of the transition from the bottomside to the E valley with which to tackle this problem.

The IRI model provides two B_0 options for describing the bottomside electron density distribution below the F_2 peak. The old option uses a table of values of B_0 deduced from profile inversion of ionograms from mid-latitude stations [Bilitza, 1990]. The new option is considered to be the better choice for the low-latitude regions [Bilitza, 1990]. The option uses Gulyaeva's (1987) model for B_0, based on the height at which the electron density has dropped to half the maximum density of the F_2 layer, $h_{0.5}$ ($N(h_{0.5}) = 0.5N_mF_2$) [Sethi and Pandey, 2001]. Both options are mainly based on data from middle latitudes with a few more data points from low and equatorial latitudes. The 12 month running mean of the sunspot number observed at the Zürich Observatory (Rz_{12}) is currently being used by the IRI model. A linear interpolation is used in solar activity up to a sunspot number (Rz_{12}) of 150. Above the sunspot number (Rz_{12}) of 150 a constant value of B_0 is assumed. For the diurnal variation IRI assumes a smooth transition from a constant daytime value to a constant nighttime value. For the table option currently no interpolation scheme is applied between the seasons, but an annual interpolation procedure was introduced for the Gulyaeva option [Bilitza, 2001].

The variability and deviations from the monthly medians of the ionospheric parameters can reach 20-40% for quiet times and even more for disturbed times (magnetic storms). Using a measured characteristic ionospheric parameter as an input in the IRI tables model can

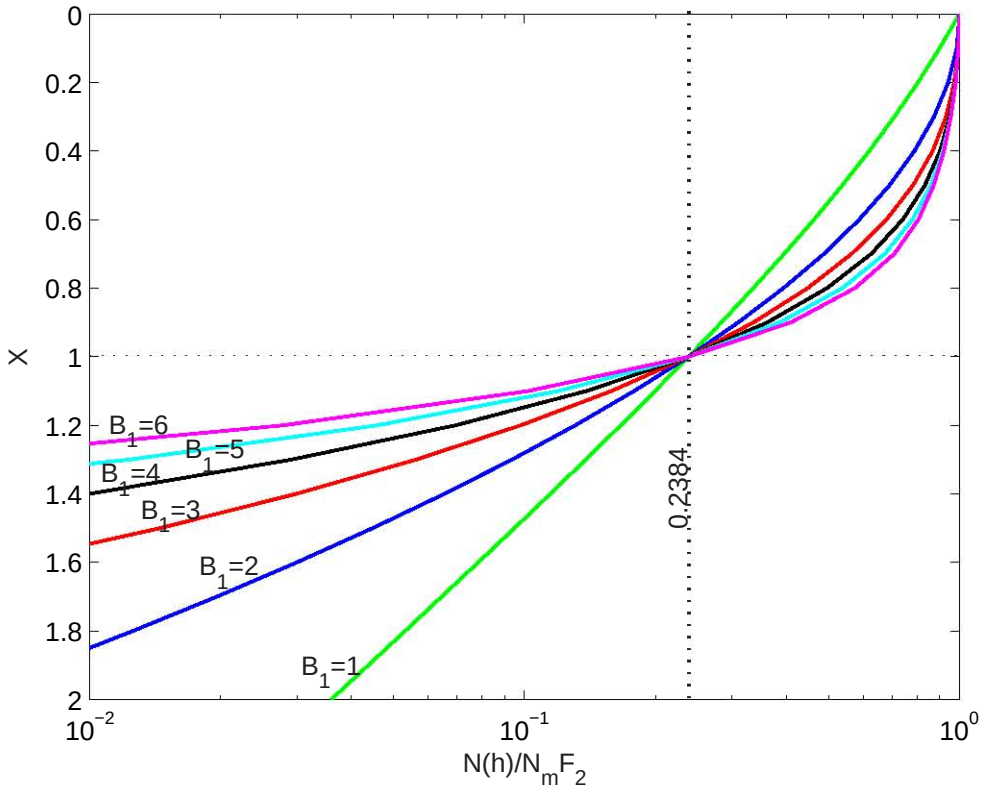

Figure 2.2: IRI function X for different values of B_1 (adopted from Reinisch and Huang, 1998)

improve the prediction of the day-to-day variability, especially for the magnetically disturbed times. Measured peak parameters can be entered by the user in the IRI model to update the electron density profiles. By so doing the electron density profile will be adapted to the observed ionospheric characteristic parameter. The updates require the user to specify the input peak parameter, the location and the time for which the IRI profile is being generated [Bilitza, 2000].

2.2.3 The F_1 layer (h_mF_1 to H_z)

The IRI-90 model for the F_1 layer is difficult to fit to actual profiles with its one free parameter, C_1 . A new functional description of the F_1 layer has been given in Reinisch and Huang, [2000]. It avoids the difficulties found in IRI-90 for the modeling of the F_1 profile. The new F_1 representation also has one free parameter, D_1, which is the F_1 layer shape parameter. The modern ionosondes used in the digisonde network automatically scale the ionograms and calculate D_1, B_0, and B_1 in real-time together with other important ionospheric parameters. A reasonable fit is obtained by using $D_1 = 2.5C_1$ [Reinisch and Huang, 2000].

The following relationship of the variation of the F_1 plasma frequency, f_0F_1 with the solar zenith angle χ, solar activity (R_{12}), and the magnetic dip latitude (Ψ) was established by Ducharme *et al.* (1971, 1973).

$$f_0F_1 = f_s cos^{\eta}\chi \tag{2.4}$$

$$f_s = \frac{f_0(f_{100} - f_0)R_{12}}{100} \tag{2.5}$$

$$f_0 = 4.35 + 0.058|\Psi| - 0.00012\Psi^2 \tag{2.6}$$

$$f_{100} = 5.348 + 0.011|\Psi| - 0.00023\Psi^2 \tag{2.7}$$

$$\eta = 0.093 + 0.0046|\Psi| - 0.000054\Psi^2 + 0.0003R_{12} \tag{2.8}$$

This model provides a critical zenith angle χ_s for the occurance probability of the F_1 layer. The F_1 layer is assumed to exist when [Bilitza, 1990]

$$\chi < \chi_s \tag{2.9}$$

where

$$\chi_s = \frac{\chi_0(\chi_{100} - \chi_0)R_{12}}{100} \tag{2.10}$$

$$\chi_0 = 49.85 + 0.35|\Psi| \tag{2.11}$$

$$\chi_{100} = 38.96 + 0.51|\Psi| \tag{2.12}$$

The height at which the bottomside IRI profile reaches the F_1 peak density, N_mF_1 is h_mF_1. The choice of the bottomside thickness parameter B_0 will affect the peak height, h_mF_1. The F region profile is connected from the F_2 layer peak, h_mF_2 down to the top of the valley using three analytical functions. In the case of no F_1 layer the profile is defined by two analytical functions [Bilitza, 1990]. The bottomside F_2 layer profile equation (2.2) is valid from h_mF_2 to h_mF_1 in the presence of an F_1 layer. When the F_1 layer is not present it is valid from h_mF_2 to $H_z = (h_mF_2 + H_{ST})/2$. The different heights for the electron density profile are shown in figure 2.3. The function for the F_1 layer is [Reinisch and Huang, 2000]

$$\frac{N(h)}{N_mF_2} = \frac{e^{-X^{B_1}}}{cosh(X)} * C_1 \left(\frac{h_mF_1 - h}{B_0}\right)^{1/2} \tag{2.13}$$

with

$$C_1 = \begin{cases} EPSTEP(18; 0.09, 0.2, 30, 10) & \text{for } |\mu| < 18 \\ EPSTEP(\mu; 0.09, 0.2, 30, 10) & \text{else} \end{cases} \tag{2.14}$$

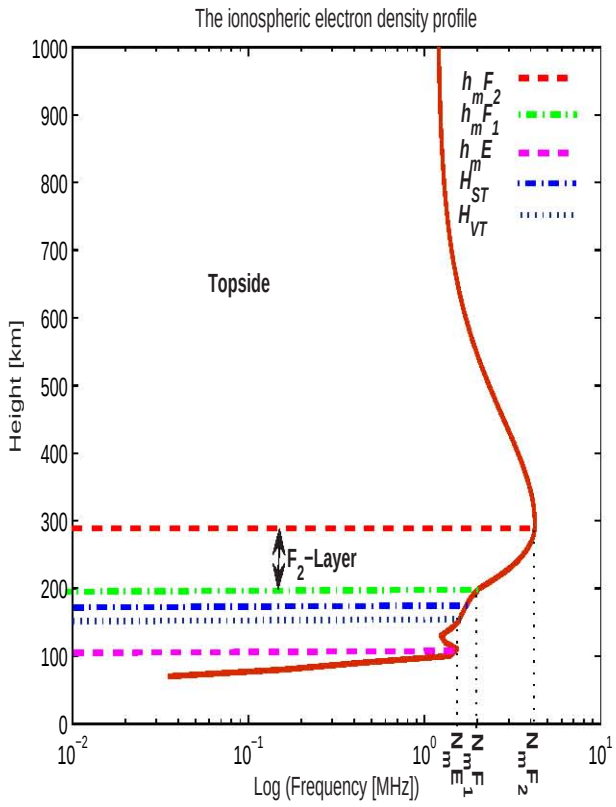

Figure 2.3: Electron Density profile showing different heights

(For more information on the function of the F_1 layer, see Reinsch and Huang (2000))

Where μ is the modified dip latitude. These are explained further in Bilitza (1990). The new F_1 layer profile extends from h_mF_1 to the top height h_{VT} of the valley. Equation (2.13) describes the profile from h_mF_1 to H_z. The height H_z is redefined as $H_z = (h_mF_1 + H_{ST})/2$, where H_{ST} is the height obtained from equation (2.13) for $N = N_mE$. The expressions for the intermediate layer, extending from H_z to H_{VT} together with the rest of the new IRI F_1 profile functions are given by Reinisch and Huang, [2000]. In this thesis, the variability of the D_1 parameter over Grahamstown, South Africa, will also be considered.

2.3 Ionospheric data

An ionospheric sounder, called an ionosonde, is used to monitor the behaviour of the ionosphere. An ionosonde is a type of High Frequency (HF) radar, and is the most commonly used ionospheric sounding device today. All signatures of the electromagnetic signals reflected from the ionosphere are measured: time of flight, wave polarization, amplitude, phase

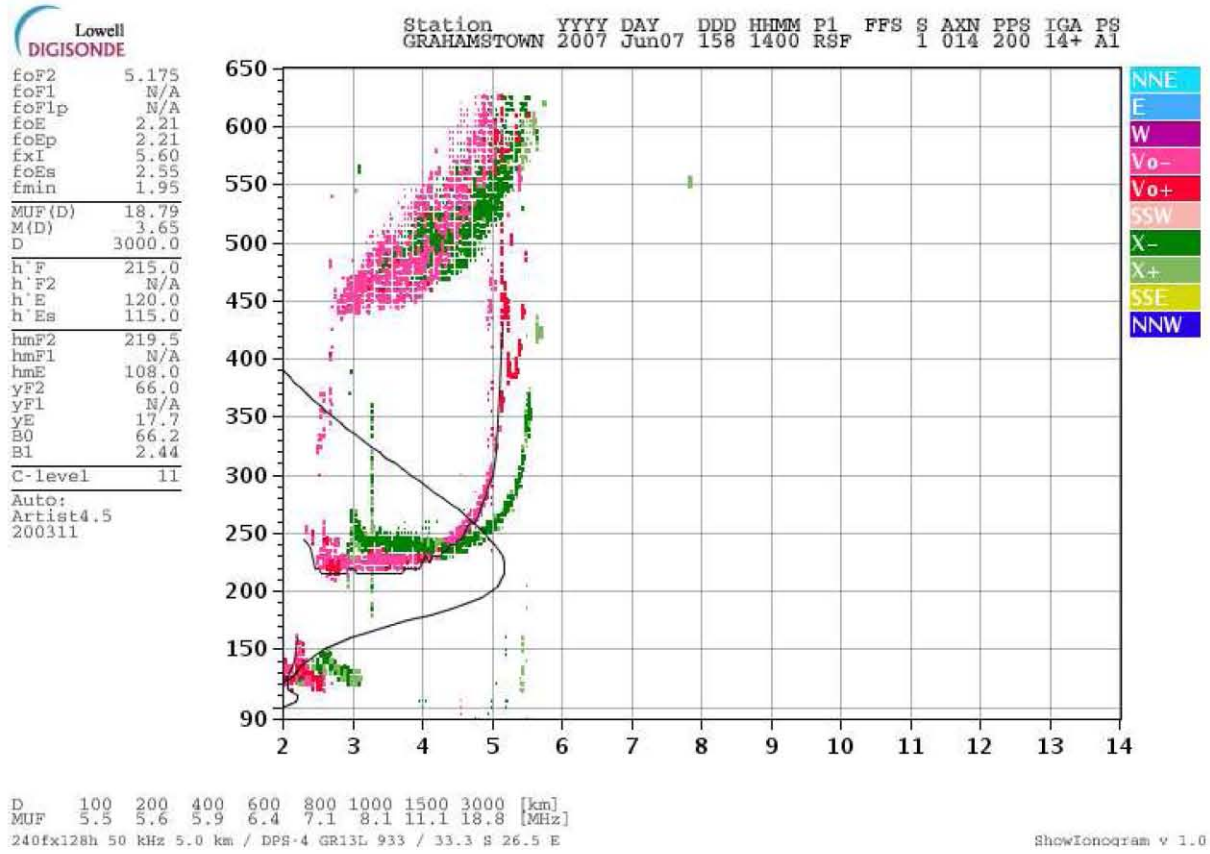

Figure 2.4: An example of an ionogram from Grahamstown

spectrum and angle of arrival. The ionosonde automatically scales the multi-parameter ionograms to provide ionospheric characteristics and electron density profiles in real-time. An ionogram is a record of the echo delay time versus frequency. The axes are easily re-calibrated to provide a graph of virtual height versus frequency which is what is observed in ionograms. An example of an ionogram from Grahamstown is shown in figure 2.4. An ionogram can be converted into an electron density profile N(h), which is a graphical representation of how the electron density varies with real height in the upper atmosphere. The relationship between the electron density and the frequency is given by equation (2.1).

Ionosondes use the principle of vertical incidence ionospheric sounding. This entails High Frequency (HF) radio waves of frequency f being sent vertically upwards. These HF radio waves are then reflected at the cut-off frequencies of the ionospheric magnetoplasma [Kohl *et al*, 1996]. To probe the E and F regions of the ionosphere the ionosonde scans from about 0.1 to 30 MHz, transmitting modulated radio waves, and receiving and analysing the ionospherically reflected echo of the signals [Kohl *et al*, 1996]. Each sounding produces an ionogram, a graph of virtual height versus frequency. Serious problems in the data quality can arise from unsatisfactory station maintenance and from errors in the autoscaling, mainly caused by high interference levels, restrictions in the frequency transmission license, and se-

vere ionospheric disturbances [Reinisch *et al*, 2003].

A digital portable sounder (DPS) which operates on a pulse sounding technique has been operating in Grahamstown since 1996. Ionospheric information for the bottomside ionosphere can be obtained from a ground-based ionosonde (DPS) as in the case of Grahamstown. The propagation of the transmitted radio wave is affected by free charges in the medium in which it is travelling. The refractive index of the medium is determined by the electron density and the magnetic field of the medium and by the frequency and polarisation of the transmitted wave. The refractive index of the ionosphere varies with height, since different layers of the ionosphere have varying electron densities. Transmitting a range of frequencies vertically upwards and measuring the time of flight for each reflected frequency allows the estimation of the densities and heights of the layers in the atmosphere. [Davis, 1998]

Each wave is refracted less by the layers in the ionosphere as the frequency is increased, hence each wave penetrates further before it is reflected. A maximum frequency is reached for the wave to be reflected when the plasma frequency of the layer is equal to the transmitted frequency of the ordinary wave. In the case of the extraordinary wave the magnetic field has an effect, therefore the reflection occurs at a higher frequency. In this thesis we are only concerned with the ordinary wave. Frequencies above the critical frequency will pass the layer without being reflected. The ordinary and extraordinary wave phenomena can be found in Davies (1990).

The technique of remote sensing by radio waves is widely used to derive information about the ionosphere. Remote sensing is the acquisition of information from the ionosphere in real-time by sensing devices. This technique detects and records the reflected wave, thereby measuring the properties of the ionosphere. The remote sensing technique is used by the vertcal sounding ionosondes to probe the ionosphere. The ionosonde data used in this study was obtained from the South African Ionospheric Data Centre webserver (http://ionosond.ru.ac.za)

The data from the sounder is automatically scaled and inverted using a software package called Automatic Real Time Ionogram Scaler with True height algorithm (ARTIST), which has an output (amongst other parameters) electron density profiles. The output from ARTIST is recorded in Standard ARTIST Output (SAO) format. The output of ARTIST is processed using a programme called SAO-Explorer to obtain the actual shape parameters. The SAO files are the ones used for the extraction of the shape parameters.

2.3.1 ARTIST-4

The DPS installed at Grahamstown provides raw real-time virtual height data, and employs ARTIST, an automatically scaling software package. The output of ARTIST includes the virtual-to-real height data conversion. There are times when ray tracing is degraded because of difficulties surrounding the real-time characterisation of the F_1 region by ARTIST. Possible shortcomings in the ability of ARTIST to characterise the F_1 region have been seen in poor real-time ray tracing results [Jacobs *et al.*, 2004].

There are three states which can be assigned to the F_1 region, namely the N, F and L states. The N state is when there is no F_1 layer (mainly nighttime), the F state is when the F_1 layer is present (mainly daytime) and the peak frequency of the F_1 layer, f_0F_1 can be determined, and finally, the L state is when the F_1 layer is present and f_0F_1 cannot be determined because the F_1 layer is shown as a ledge rather than a cusp on the ionogram. The L-condition exists as a transition state between the N state and the F state (mostly in the mornings and evenings). ARTIST makes no allowance for the L-condition state even though there is evidence of significant departures in the real-height profiles, hence the need to manually re-scale the DPS ionograms for the years 2000, 2004 and 2005. Manually re-scaling the ionograms helps recover the value of f_0F_1 which could be lost when only the automatic scaling is used. The L-condition is more likely to occur around sunset and sunrise, but it can also be present during daytime more especially in the winter [Jacobs *et al.*, 2004]

ARTIST automatically scales the ionograms and generates a **.SAO** file for each ionogram. The SAO file contains all the parameters and information pertaining to that ionogram as determined by ARTIST. The manual editing is done using a programme called SAO-Explorer. Both the raw data (files with the extension **.RSF**) and SAO files (with the extension**.SAO**) are required to manually edit the ionogram. SAO-Explorer allows the processing of many ionograms simultaneously, so a time interval of a month was chosen for this procedure. All the raw files and the SAO files for a particular month were copied to one directory, making sure that for each SAO file there is a corresponding raw file. At this point the SAO-Explorer was launched and the manual scaling done. For more information on the SAO-Explorer visit the SAO-Explorer User's Guide at $http://ulcar.uml.edu/SAO-X/UsersGuide.html$ and for information on reprocessing digisonde data with ARTIST-4 software visit $http://ulcar.uml.edu/ARTIST4/Offline.html$. The extraction of the actual shape parameters is achived by loading only the SAO files on the SAO-Explorer. The resultant files have the shape parameters together with the time and the date on which the data was recorded. The instructions on how to extract the parameters from the SAO-Explorer can also be obtained from the SAO-Explorer User's manual.

2.4 Conclusion

The IRI model was developed using data from reduced number of ionospheric stations, but it is the best available global model to date. This makes the model deficient in predicting the IRI shape parameters over some parts of the world. In this thesis the IRI-2001 model ionospheric shape parameters will be compared with the ones analysed in this study and reasons why there may be any differences discussed. An evaluation of the functions which are used in the construction of the IRI model to represent the diurnal, and latitudinal variations will also be done. The IRI F_1 profile which is given by equation (2.13) will be looked into and its advantages and/or disadvantages will be discussed.

Chapter 3

Variability of the IRI shape parameters

3.1 Introduction

This chapter presents the description of the data used in this study, the procedure and methods undertaken to extract the parameters, and an investigation into the variability of the IRI shape parameters over Grahamstown, South Africa. Finally, the variability of the IRI shape parameters are compared with the IRI-2001 model. The data set comprising 4 years (2000, 2004, 2005 and 2006) was used for the determination of the variability of the shape parameters. The 2000 data represents data near the solar maximum and the 2005 data represents data near the solar minimum. The data for 2000, 2004 and 2005 was sampled at 30 minute intervals and manually edited using the SAO-Explorer version 3.4.02*b*, whilst the data for 2006 was sampled at 15 minute intervals and was not manually edited. The different sampling intervals arose from the different program schedules for those years. The profiles for the months December, March, June and September will be presented in this chapter, representing the summer, autum, winter and spring periods respectively.

3.2 Data used

A total of 11 years (1996 to 2006) of Grahamstown ionosonde data was used in this study. Four years (2000, 2004, 2005 and 2006) from the data base was used for investigating the variability of the IRI parameters. The 2000, 2004 and 2005 data was manually edited using SAO-Explorer and was analysed for the diurnal and seasonal variations. The rest of the data was not manually edited, but only automatically scaled by ARTIST-4. The sampling of the

data was as follows: 1996 to 1999 at 1 hour intervals, 2000 to 2005 at 30 minute intervals and the 2006 data at 15 minute intervals.

3.3 Methodology

The shape parameters (B_0, B_1 and D_1) used in this study were obtained by converting the recorded ionograms (after manualy editing) for Grahamstown, South Africa ($33.3\,^{\circ}S$,$26.5\,^{\circ}E$) to true height electron density profiles, by using the inversion algorithm NHPC which is embedded in the SAO-Explorer software package [Lee and Reinisch, 2006]. The obtained true height electron density profiles are fitted, using a least-square-fitting approach and using the observational N_mF_2 and h_mF_2 value as the anchor point, with equation (2.7) by means of a FORTRAN subroutine in the package. The profile fitting is made from h_mF_2 to $h_{0.24}$ if no F_1 layer exists, or to the F_1 peak if an F_1 layer occurs [Zhang *et al*, 2007]. For better evaluation, the IRI profiles are compared with monthly median representative profiles of the data rather than with individual profiles, since the IRI model represents an average ionosphere. The predicted B_0, B_1 and D_1 IRI values were obtained from the latest version of the ionospheric model (IRI-2001). For the B_0 parameter,the IRI offers two options, namely the Gulyaeva's model [Gulyaeva, 1987] and the B_0-tables method [Bilitza *et al*, 2000]. In order to compare the observational variations and the IRI-2001 in detail, the observed monthly median values together with the IRI-2001 predicted values were plotted on the same graph. For the B_0 parameter two predicted curves for either of the two options were plotted on the same axis.

Each data file for the years 2000, 2004 and 2005 was sampled at 30 minute intervals. The periods analysed covered all hours of the day for 365 days for each year analysed. The files had the information on all the parameters in the ionosphere together with the date and the time at which the data was recorded. Only the parameters needed for this study were extracted because the SAO-Explorer gives the user a choice of the parameters to be extracted. These files were then saved and exported to Excell where the initial handling of the data was done. This included the exclusion of outliers from the data base. Matlab programmes were developed for the determination of the monthly median values of the parameters, annual values for a particular time and the final plotting of the graphs.

3.4 Results

3.4.1 Variation of B_0

Diurnal and seasonal variation of B_0

The diurnal variation of B_0 for different seasons in 2000, 2004 and 2005 is presented in the form of universal time versus B_0 graphs. Four months are used to represent the four different seasons of the year; March representing autumn, June representing winter, September representing spring and December representing summer. The IRI-2001 normalised profiles were generated using both the methods offered by the IRI for the prediction of B_0. The IRI-2001 predictions were obtained without using the peak frequency of the F_2 layer, f_0F_2. Figures 3.1, 3.2 and 3.3 show the diurnal variations of the thickness parameter of the F_2 layer, B_0 at Grahamstown for the monthly median observed values (indicated as "Meas" on the graphs) together with the two options of the IRI-2001 model. Each panel represents a different season of each year. Figure 3.1 represents the variations in 2000, figure 3.2 those for 2004 and figure 3.3 those for 2005. Both the IRI-2001 tables method (indicated as "IRI" on the graphs) and the Gulyaeva (indicated as "Guly" on the graphs) option are plotted together with the observational monthly median representative results.

Observational results are represented by red stars ($*$), the Gulyaeva option is represented by black addition signs ($+$) and the IRI-2001 tables method is represented by blue diamonds ($\blacklozenge$) in the figures 3.1, 3.2 and 3.3. From the observational results it can be seen that there is a well-defined seasonal and diurnal variational pattern. In the diurnal variation the thickness parameter of the F_2 layer B_0 has its maximum values during daytime and its minimum values at nighttime. The seasonal variation shows minimum values for B_0 in the winter (June) followed by spring (September), then autumn (March) and a maximum in summer (December). The graphs also show that the monthly median observed values are generally higher for high solar activity and smaller for low solar activity. An interesting feature on the graphs is the sudden drop in the thickness parameter at around sunrise and sunset. This feature is observable during all the seasons and at times of low and high solar activity. The graphs show that the feature is more pronounced for the high solar activity years. The sudden drop in B_0 is represented by the prediction in the Gulyaeva option of the IRI model.

There is a general increase at around sunrise (around 04h00 UT in summer, 05h00 UT in spring, 05h00 UT in autumn and 06h00 UT in winter) in the B_0 parameter. The increase continues until around local noon (10h00 UT) for all the seasons excluding winter. In winter

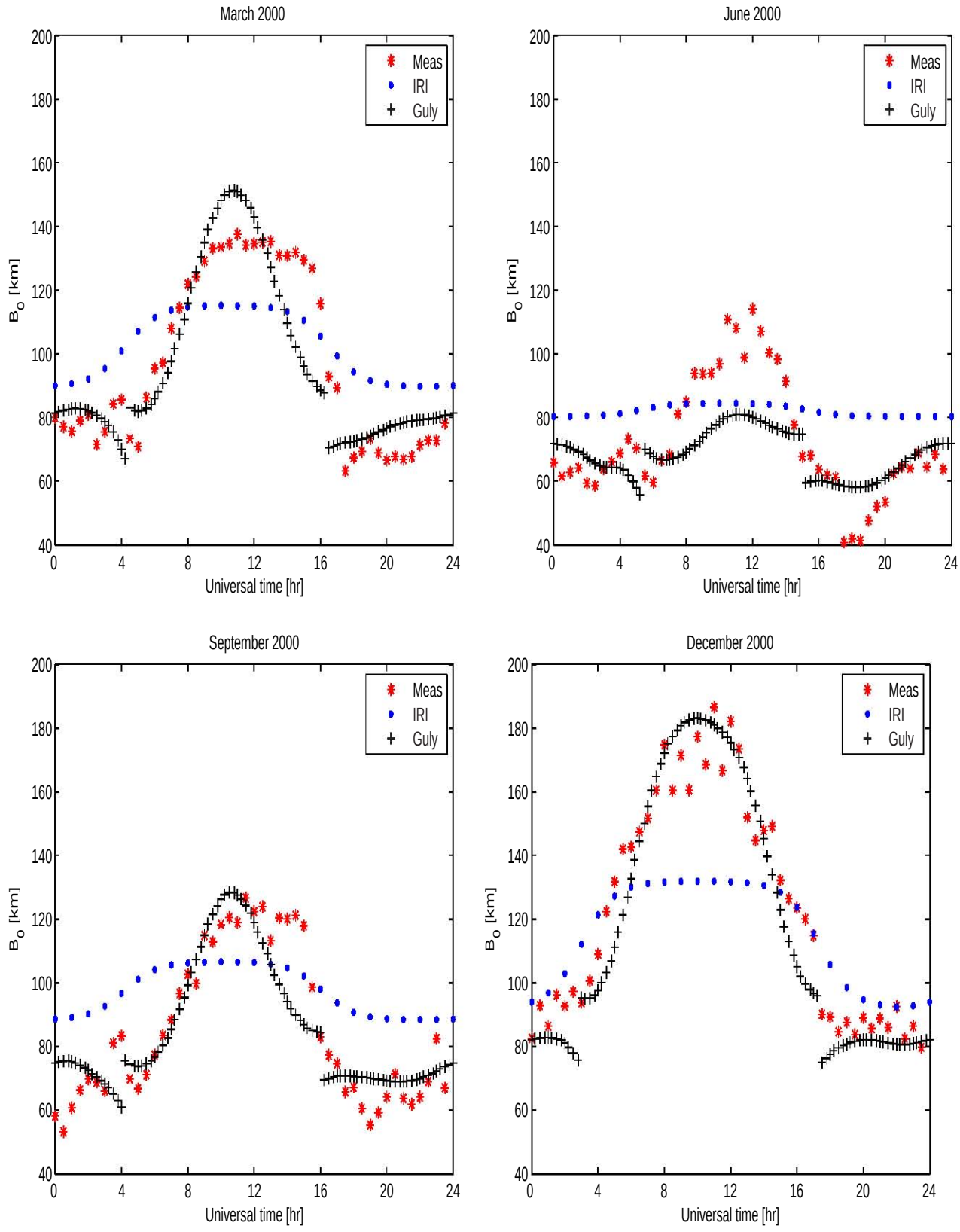

Figure 3.1: Diurnal variations of the B_0 parameter over Grahamstown in 2000

the increase continues until around 14h00 local time (12h00 UT). This increase could be due to enhanced solar radiation during the daytime. There is a general drop in the thickness

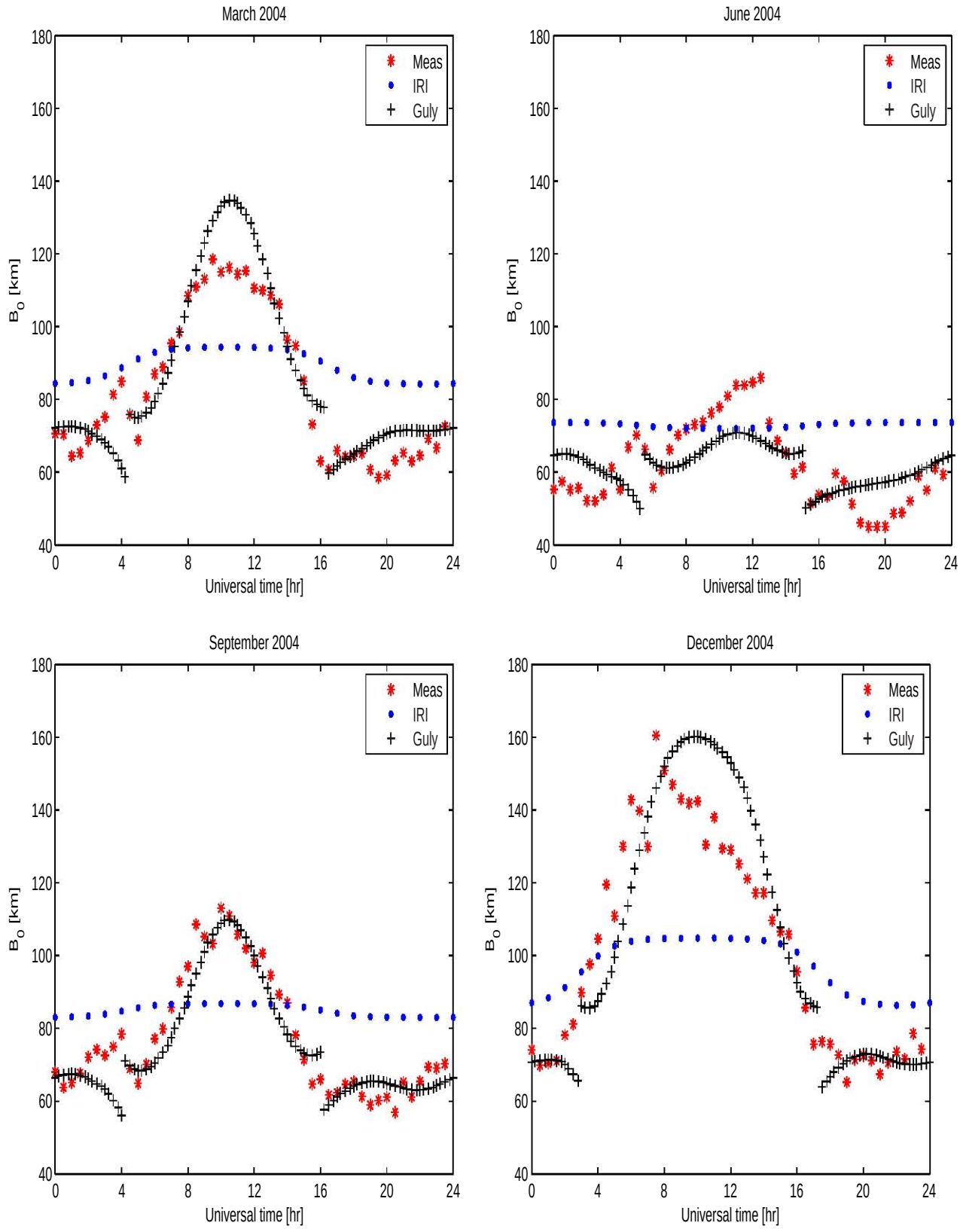

Figure 3.2: Diurnal variations of the B_0 parameter over Grahamstown in 2004

parameter at around 22h00 LT (20h00 UT). This is more pronounced in the winter for the different solar activities. The drop is followed by an increase in B_0 which could be an indica-

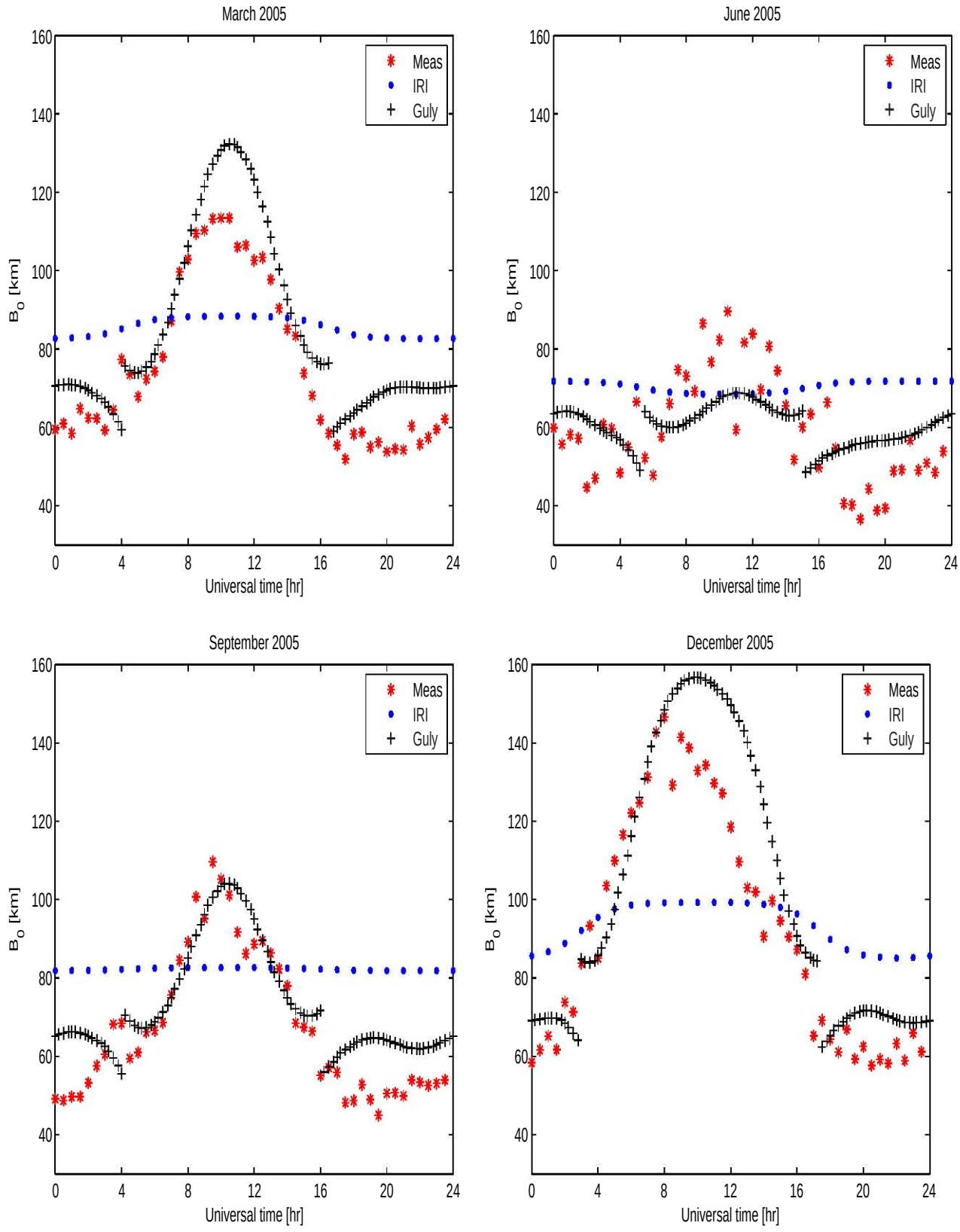

Figure 3.3: Diurnal variations of the B_0 parameter over Grahamstown in 2005

tion of an upward velocity. For all three years analysed, the Gulyaeva option overestimates B_0 during autumn and underestimates B_0 in winter for the period 10h00 to 16h00 local time

(08h00 to 14h00 UT). In the summer the Gulyaeva method is accurate for the prediction of the year 2000 (high solar activity) and the Gulyaeva's peak for the years 2004 and 2005 (low solar activity) is shifted to around two hours later. The prediction by the Gulyaeva option is inconclusive for the night predictions in all the seasons and for the different solar activities. The IRI-2001 tables option underestimates B_0 during the day hours and overestimates B_0 for the nighttime for all the seasons and different solar activities. For the diurnal variations the Gulyaeva's option is definitely an improved method for the prediction of B_0.

Annual variation of B_0

In the investigation of the annual local noon variation, data for the years 2000 and 2006 was used. The observational results show a well-defined annual variation pattern with the minimum B_0 values in the winter time and the maximum B_0 values in the summer as seen in figure 3.4. The variation of the B_0 parameter is a smooth decrease in the thickness parameter reaching its low in winter (June) and then a gradual increase reaching its maximum in summer (December). It is clear from the plots that the IRI-2001 tables option does not accurately represent the annual variation. The method assumes a constant value for a particular season since no interpolation scheme has been applied between the seasons. On the other hand, the Gulyaeva option obtains the correct trend in the annual variation. For the 2000 observations the Gulyaeva's option overpredicts the B_0 parameter in the summer (December, January) and underpredicts the B_0 parameter in the winter (June, July). For the 2006 observations, the Gulyaeva option slightly overpredicts the B_0 parameter for the summer months and slightly underpredicts the parameter for the winter months. The tables method underpredicts B_0 for both the years. It can be said that the Gulyaeva option is more accurate in its prediction of the annual variation for the low solar activity years. The Gulyaeva method clearly represents the observed values more accurately than the tables option for the Grahamstown data.

The local midnight annual variation shows small fluctuations in the average thickness parameter throughout the year, as illustrated in figure 3.5. Only the 2006 graph is presented, since the features of the other years are similar to the features in the 2006 graph. The graph shows that the local midnight annual variation is more or less constant throughout the year with slightly higher values of B_0 during the summer. The IRI-2001 tables option overpredicts the annual local midnight B_0 variation and assumes constant B_0 values for each season. Unlike its prediction of the local noon annual variations, the Gulyaeva option overpredicts the B_0 variation throughout the year and does not have the smooth annual variation. The Gulyaeva method is still the better option for the prediction of the local midnight B_0 annual

variation for Grahamstown's data.

3.4.2 Variation of B_1

Diurnal and seasonal variation of B_1

The analysis for the shape parameter of the F_2 layer, B_1 was completed for the same period as for B_0, i.e. 4 months of the years 2000, 2004 and 2005. The IRI offers one method in the prediction of B_1, which is the tables method. Figures 3.6, 3.7 and 3.8 shows the diurnal variations of B_1 over Grahamstown for the monthly median observed values together with the IRI-2001 model predictions. Figure 3.6 shows the diurnal variation of the B_1 parameter in 2000, figure 3.7 in 2004 and figure 3.8 in 2005. The red stars ($*$) represent the observed values and the blue diamonds ($\blacklozenge$) represent the predicted values for B_1 by means of the IRI-2001 tables method. The IRI-2001 predicted B_1 values are plotted on the same axis with the monthly median observed B_1 values for easier comparison.

The plots for the B_1 diurnal variation show that there is a welldefined diurnal variation. The shape parameter is at its minimum during the day and reaches its maximum at night. The lowest values of B_1 are found in summer, whilst the highest values are found in winter. There seems to be no clear correlation of the variability of B_1 and the solar activity, but the lowest values of B_1 were obtained for the year 2000. The plots also show an interesting feature between 03h00 UT and 04h00 UT in the morning and at around 20h00 UT in the evening. The shape parameter suddenly increases to a maximum before decreasing. This feature is observed for all seasons and levels of solar activity. The feature is not as well defined in the summer mornings as compared to other seasons and other times.

There is a general decrease in the shape parameter at around sunrise until it reaches a minimum and stays more or less constant until around sunset, when it suddenly increases. The IRI-2001 method generally performs well when predicting B_1 for autumn (March) and spring (September) during the day hours for the different years. For all three years the IRI-2001 overpredicts the shape parameter during the day in the summer. The prediction by the IRI for the daytimes in winter is not good during low solar activity. For all the years and seasons the IRI-2001 underpredicts the B_1 shape parameter during the night.

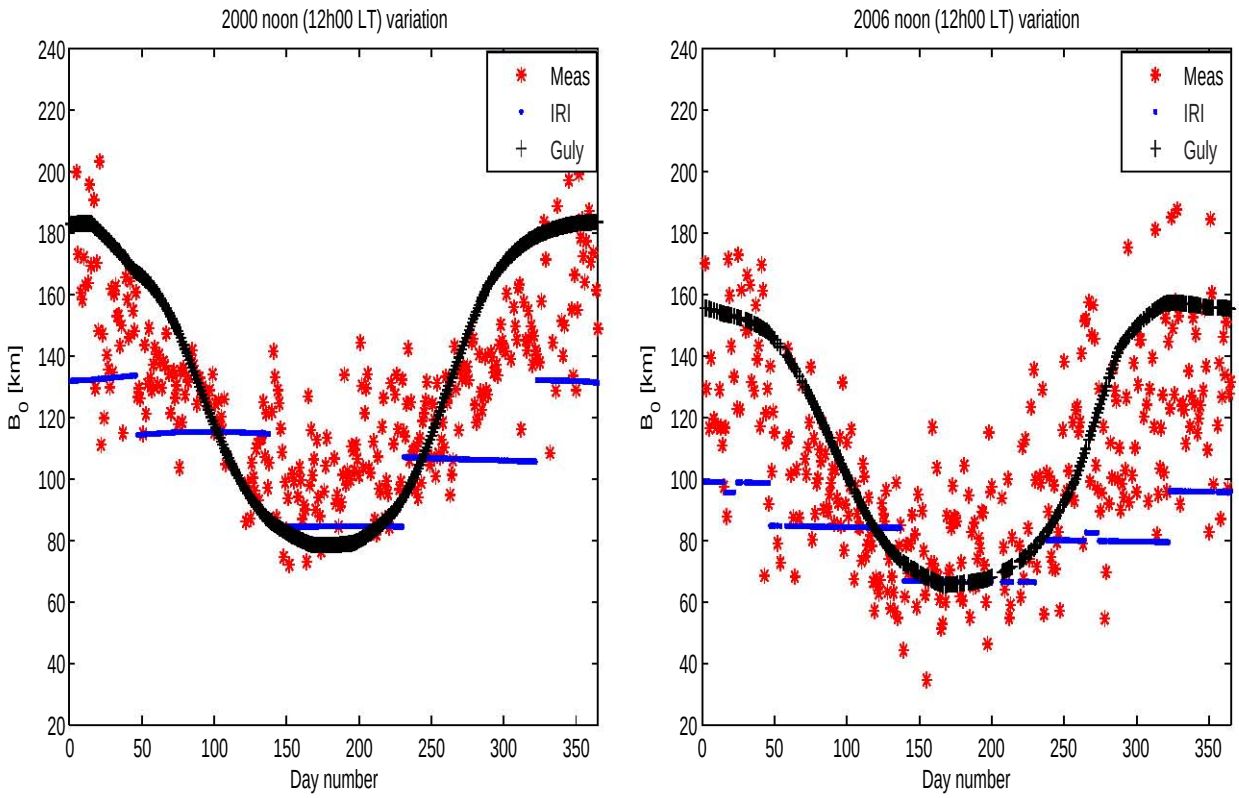

Figure 3.4: Graphs for the noon (12h00 LT) annual B_0 variation over Grahamstown for 2000 and 2006

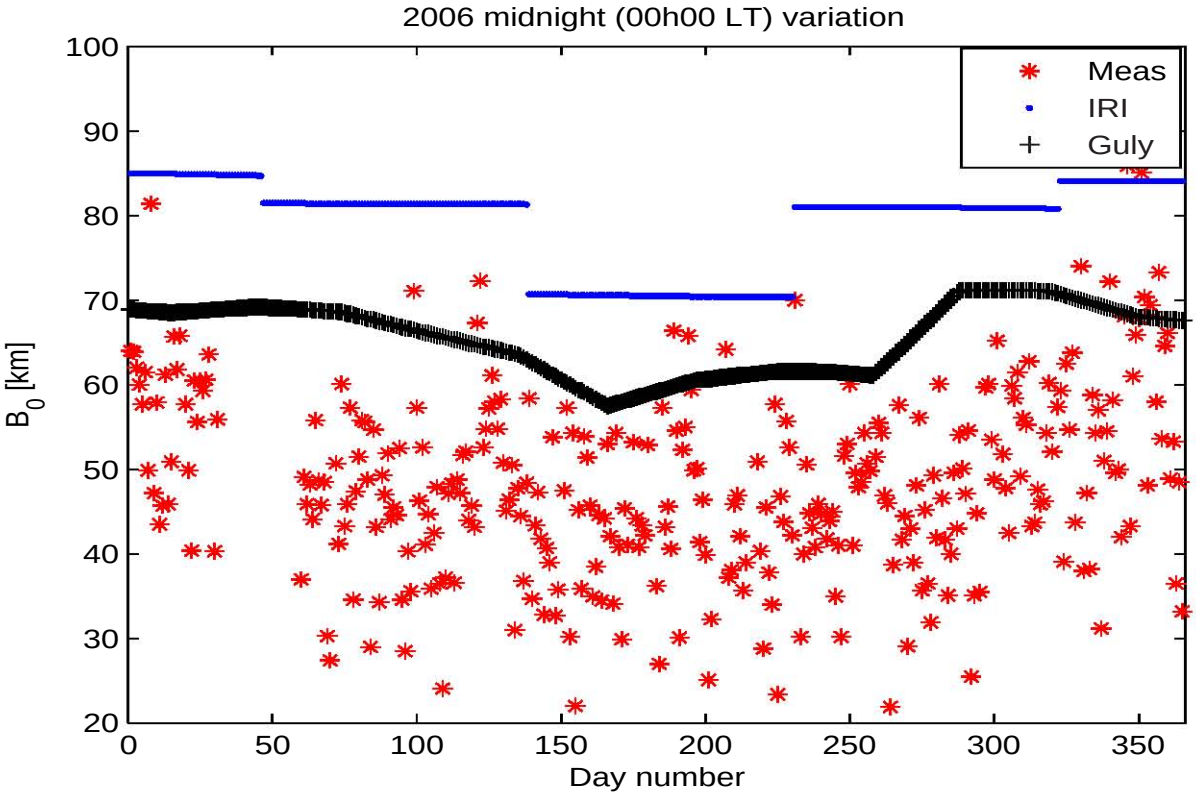

Figure 3.5: A graph for the 2006 midnight (00h00 LT) annual B_0 variation over Grahamstown

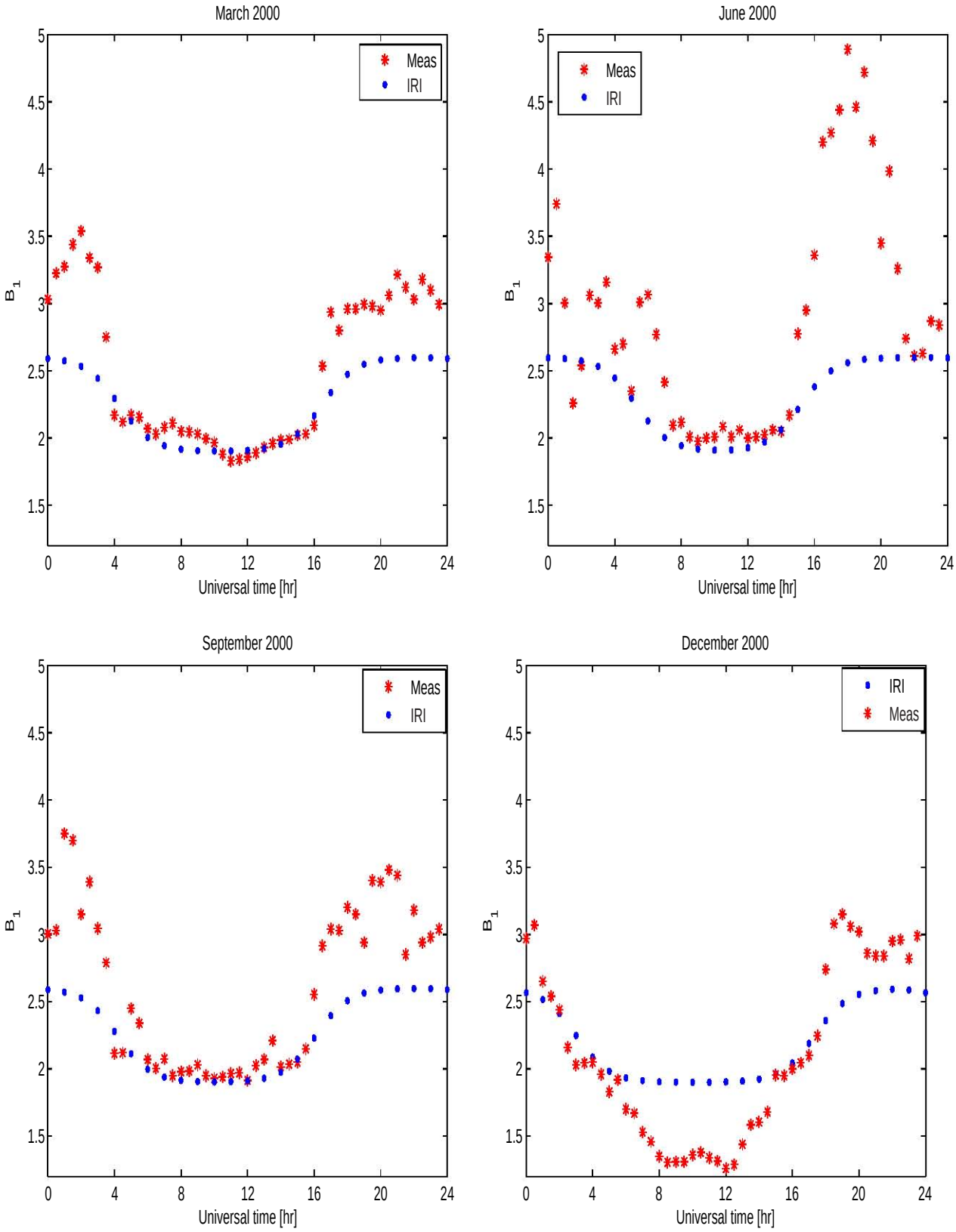

Figure 3.6: Diurnal variations of the B_1 parameter over Grahamstown in 2000

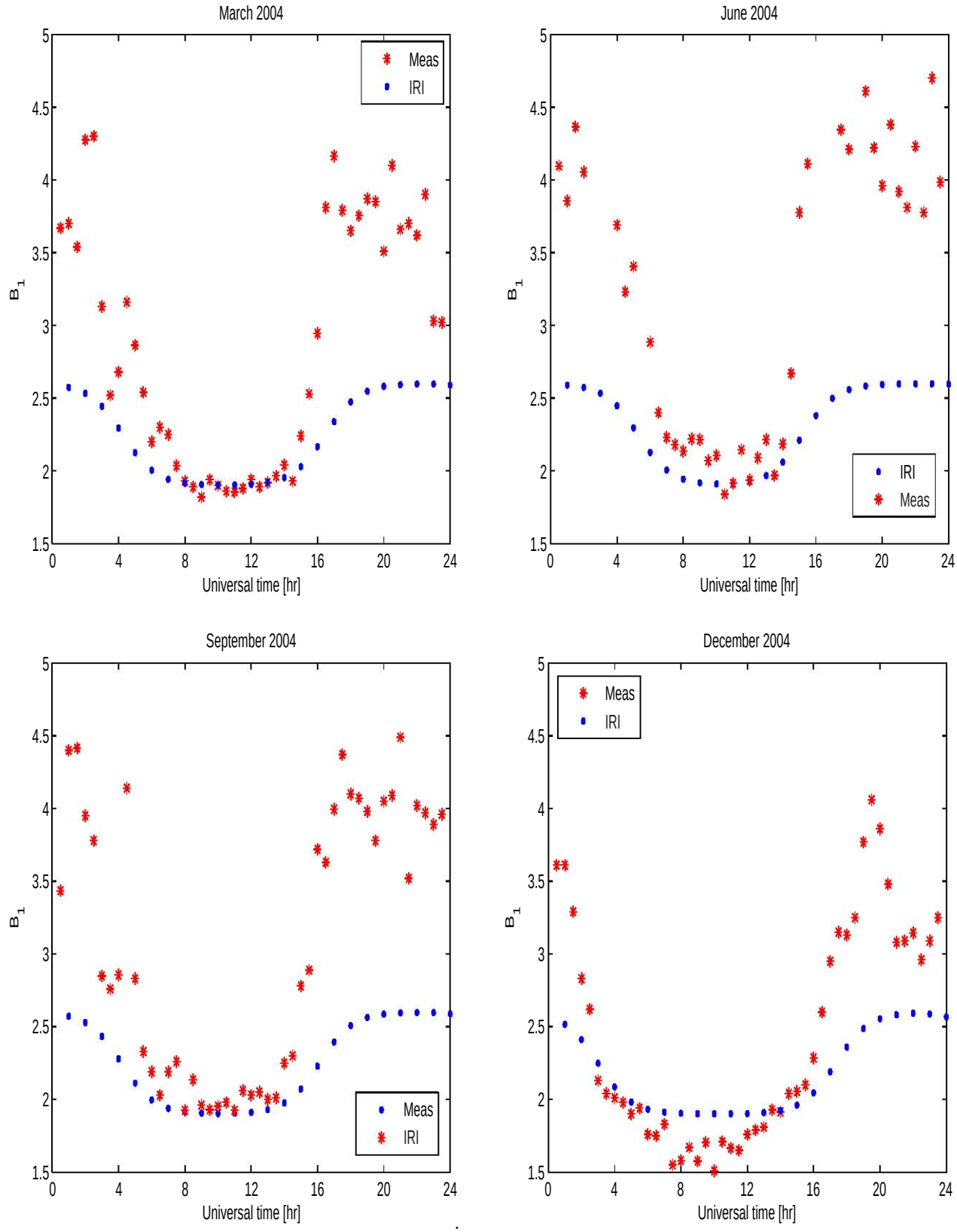

in

Figure 3.7: Diurnal variations of the B_1 parameter over Grahamstown in 2004

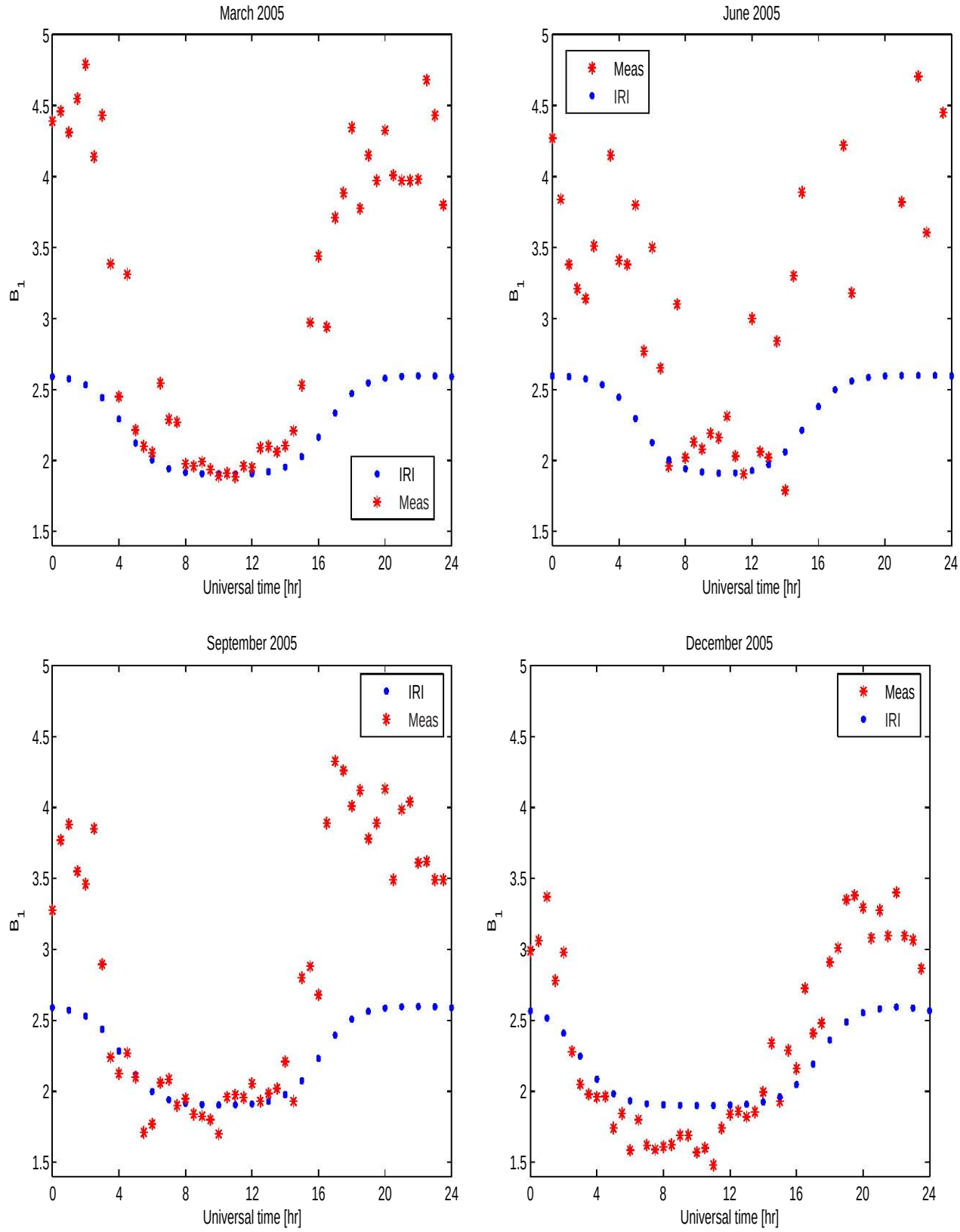

Figure 3.8: Diurnal variations of the B_1 parameter over Grahamstown in 2005

Annual variation of B_1

In the investigation of the annual variation, data for the year 2006 was used. Figure 3.9 shows the local noon annual variation of the shape parameter B_1. The observational results are inconclusive. The spread of the observational results is almost the same throughout the year. There seems to be a small cluster of the observational results above the average during the winter. The shape parameter of the F_2 region varies between 1 and about 3 at midnight. A similar pattern was noticed for the other years. The prediction by the IRI gives the same value of B_1 for the whole year. The midnight annual variation was also inconclusive. The IRI-2001 tables method underpredicts B_1 at midnight for all the seasons and different solar activities.

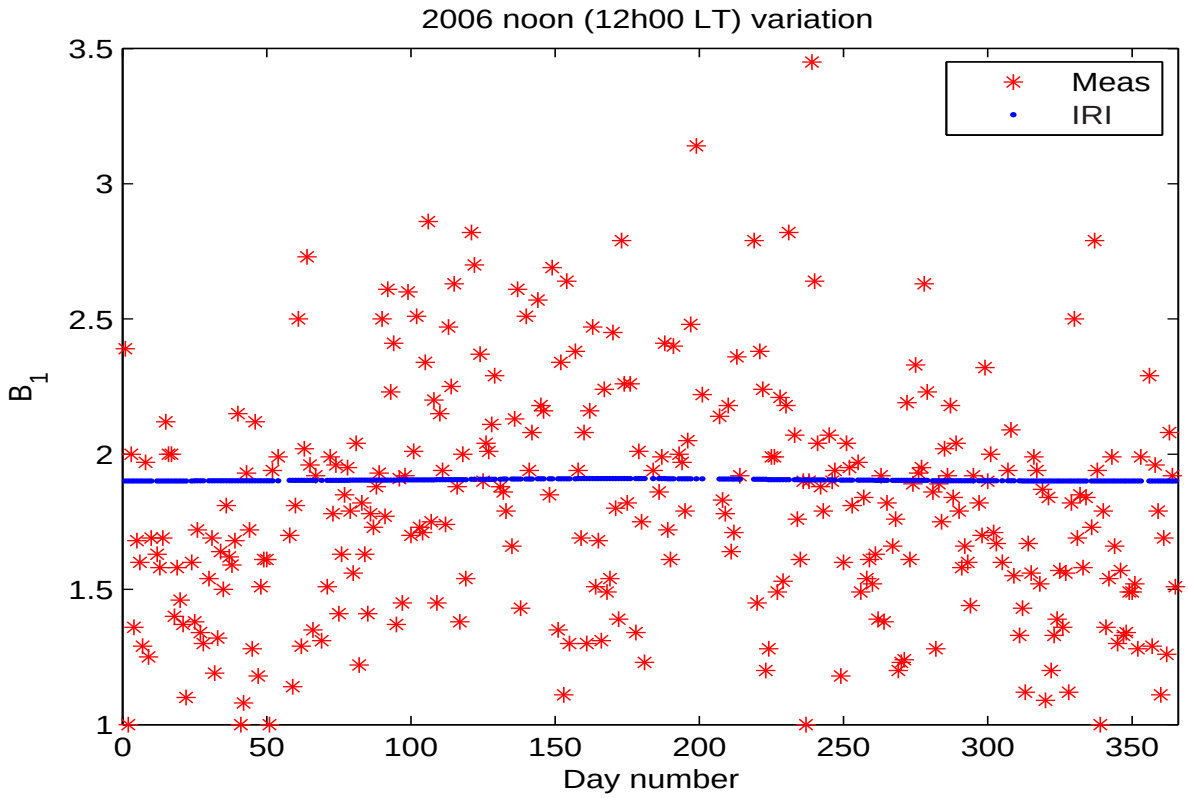

Figure 3.9: A graph for the 2006 noon (12h00 LT) annual B_1 variation over Grahamstown

3.4.3 Variation of D_1

Diurnal and seasonal variation of D_1

An analysis for the shape parameter of the F_1 layer, D_1 was undertaken for the years 2000, 2004 and 2005. In the case of D_1 there is only one IRI prediction from the IRI-2001 tables method. The plots representing the prediction from the IRI-2001 model and the observational monthly medians are shown in figures 3.10, 3.11 and 3.12. Observational results are represented by red stars (*), whilst the IRI-2001 model predictions are represented by blue diamonds(♦).

There is a clear diurnal variation of the D_1 parameter with the maximum values found at around midday for all the seasons and all the years. The plots show that D_1 is always zero at night, since there is no F_1 layer present at night. There is also a clear seasonal variation in D_1 with the lowest values for D_1 during the winter. In the winter D_1 is found for only a few hours. It can be seen that in winter D_1 is available for longer hours during low solar activity years as compared to the year 2000, which was a high solar activity year. For all the years D_1 is available for most of summer, with the hours of availability extending from about 04h00 UT until about 16h00 UT for all years analysed. During the winter D_1 was found to be available between about 08h00 UT and 12h00 UT for the year 2000, and between about 07h00 UT and 13h00 UT for the years of low solar activity. For autumn and spring it was found that D_1 is present from about 07h00 UT to 14h00 UT for the year 2000 and from about 06h00 UT to about 15h00 UT for the years of low solar activity.

The IRI-2001 tables model underpredicts D_1, with the greatest deviations found in the summer for the years of low solar activity. The IRI-2001 model does well in realising that D_1 is only available for short periods during the winter and longer periods during the other seasons.

Annual variation of D_1

The plots of the annual D_1 variation will not be presented here, because there is no clear variational pattern to be observed. There seems to be a problem in the extraction of the D_1 parameter. The annual variation D_1 was investigated. However, due to the problems with the D_1 data it was not possible to observe any real trends in the data. The annual D_1 variation will be presented in the next chapter.

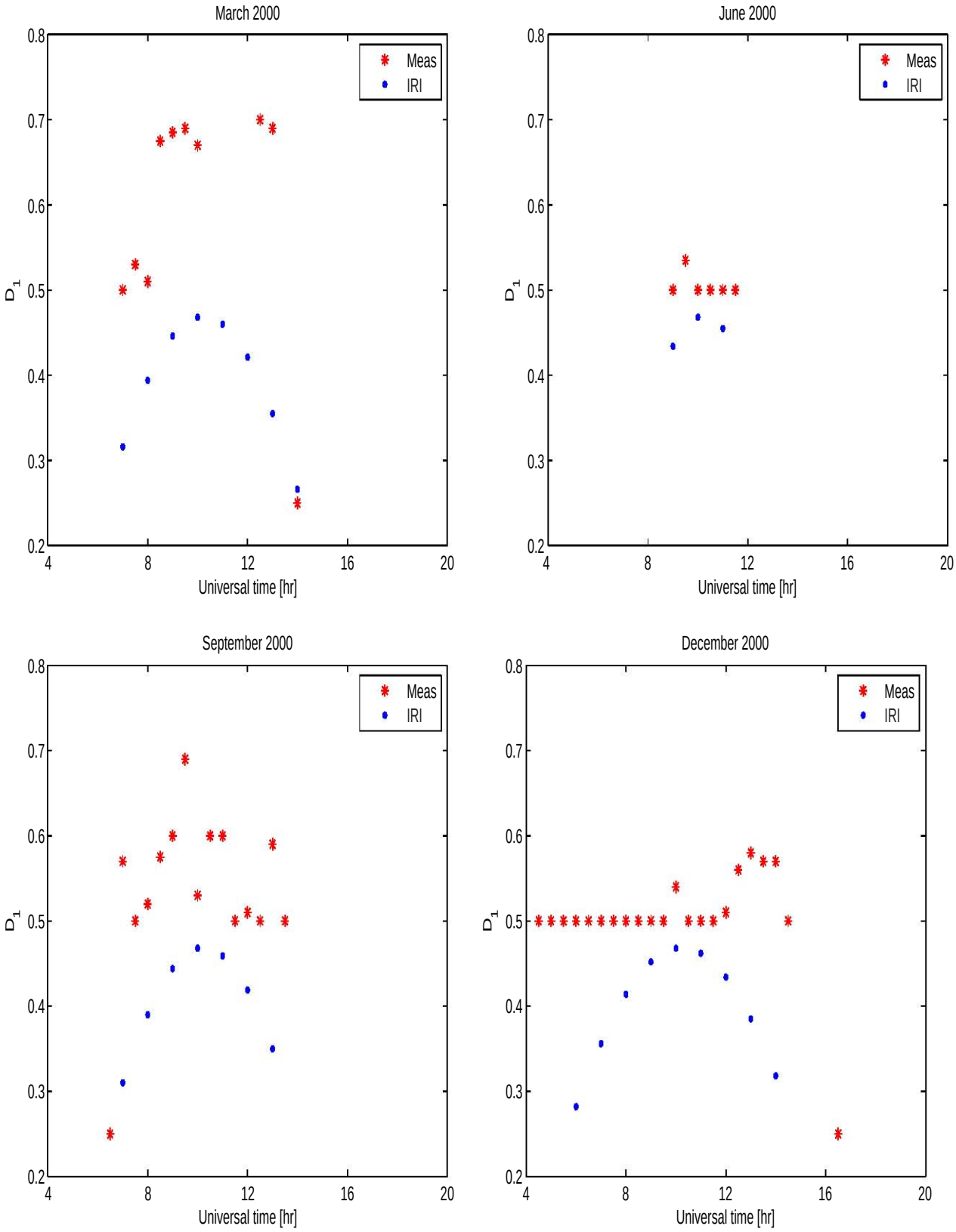

Figure 3.10: Diurnal variations of the D_1 parameter over Grahamstown in 2000

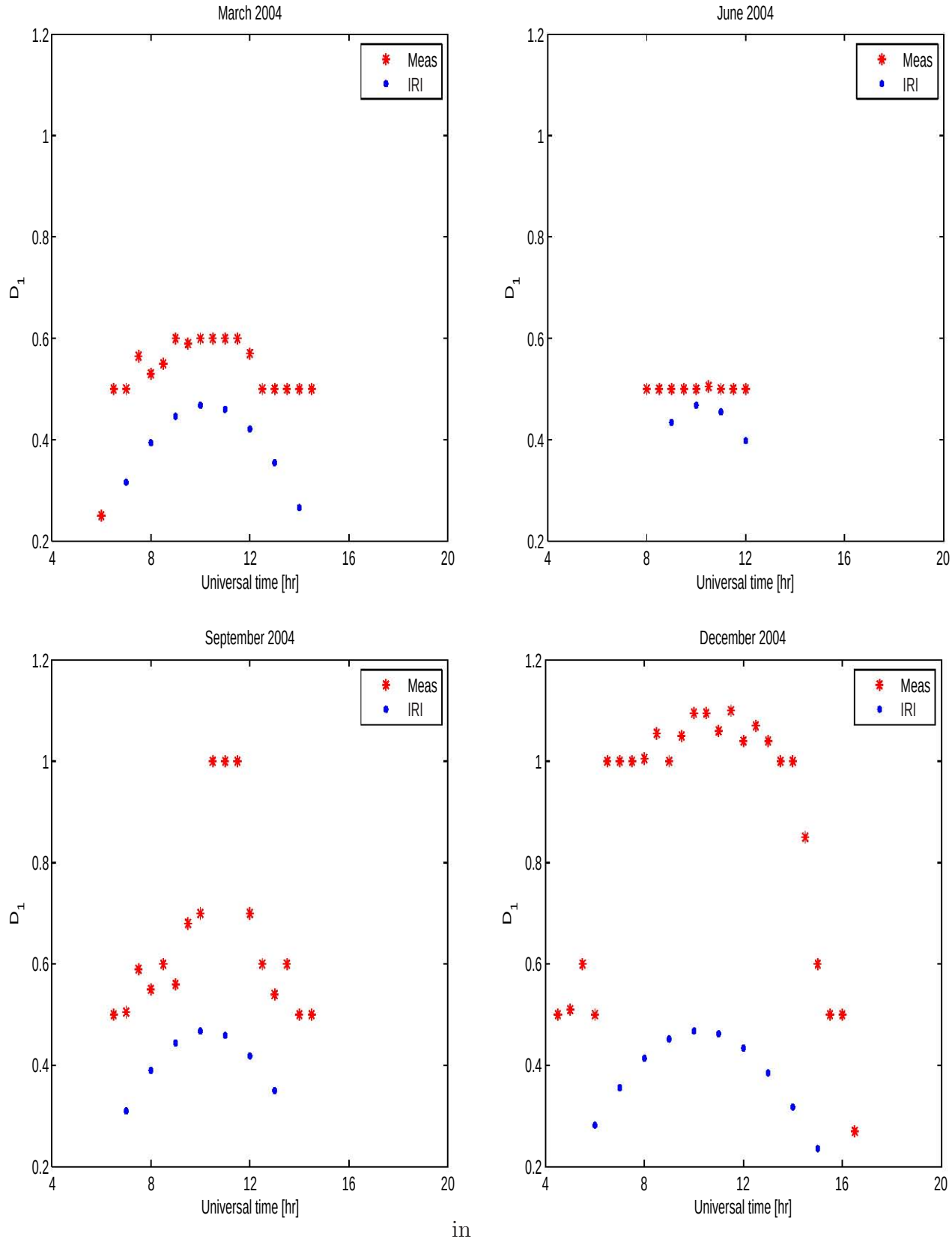

in

Figure 3.11: Diurnal variations of the D_1 parameter over Grahamstown in 2004

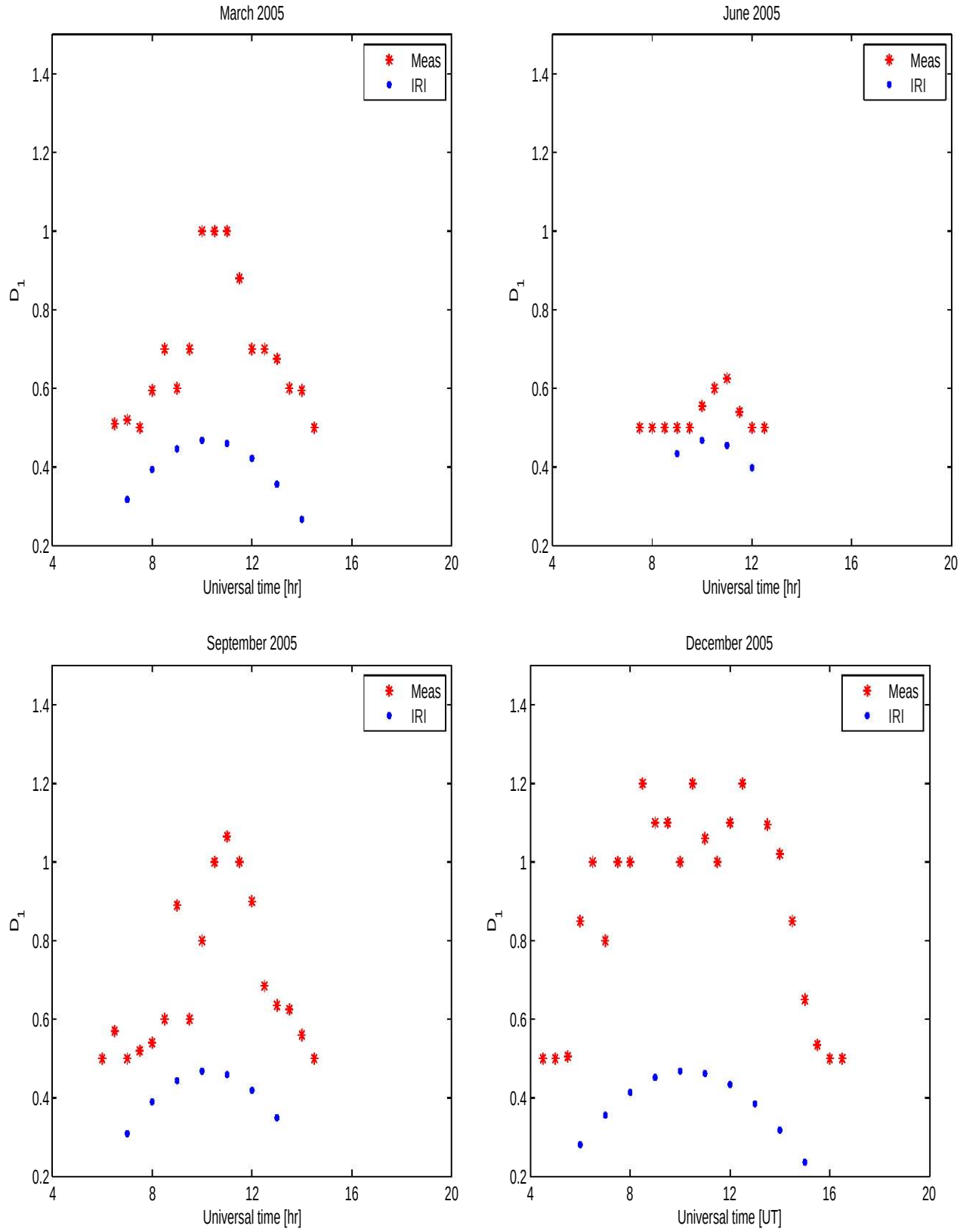

Figure 3.12: Diurnal variations of the D_1 parameter over Grahamstown in 2005

3.5 Conclusion

Comparisons between the IRI-2001 model and the monthly median observational values show that there are some deviations in the IRI-model from the observational data. The annual prediction of B_1 and B_0 by the IRI-2001 tables method needs to be improved or replaced by an alternative method for the model to more accurately represent the shape parameters. The Gulyaeva option of the IRI appears to be more accurate at the B_0 parameter prediction.

Chapter 4

Neural Network Modeling

4.1 Introduction

What follows is a brief historical overview of Neural Networks (NNs), the tool that was used to investigate a preliminary alternative model for the shape parameters of the ionospheric electron density profile. The first models using neural networks were developed around 1943 on the basis of the understanding of neurology and made several assumptions about how neurons work. These models were based on simple neurons which were assumed to be binary devices with fixed thresholds. Around 1954 scientists and engineers working with neural networks worked in close collaboration with neuroscientists and the interaction culminated in the development of modernday neural networks. The idea of neural networks was then applied by psychologists and engineers who also contributed immensely to the growth in the use of neural networks. Neural networks were used to simulate the architecture of the brain. Interest in neural networks grew after the development of the Perceptron, which could learn and associate a given input to a random output unit. During the 1960's only a few scientists continued their work on neural networks. A number of these scientists were working on developing neuromorphically based computational methods for pattern recognition [Stergiou and Siganos, 1996]. The re-emergence of interest in neural networks came from progress made during the late 1970's and early 1980's. This renewed interest can be attributed to a number of factors, including improved training techniques for the more complicated network architectures and the availibility of high-speed digital computers. These made the simulation of neural processes more feasible [Fausett, 1994]. Today interest in and funding for neural networks have brought about significant progress in the field.

4.2 Neural Networks

Artificial Neural Networks (ANN's), often called Neural Networks (NN's), are information processing systems inspired by biological nervous systems, such as the brain. These are made up of a number of interconnected processing elements (neurons) which work together to find a particular solution. ANN's, like any other biological nervous system, learn by "example". Each ANN is set up for a specific application, e.g. pattern or data recognition which can be achieved after a learning/teaching process. The learning involves adjustment of the weights of the signals at the connections between the neurons. Neural Networks (NN's) can be said to be a kind of multiprocessor computer system. This system uses simple processing elements, simple scalar messages, has interconnected elements and adaptive interaction between the elements.

One can say that ANN's are based on the following assumptions [Fausett, 1994]:

1. Processing of information is done with the neurons.
2. Neurons are connected by links which pass the signals.
3. Each connection link has a weight associated with it.
4. An activation function is applied to the net input to each neuron.

NN's can be used to extract patterns and detect trends which might be too complex for humans or other computer techniques. Modeling the way the brain functions to perform a particular task can be achieved by a NN machine. The machine can perform this task by means of a learning or training process. The main function of learning is to adjust the weights of the NN to achieve a desired design aim [Haykin, 1994]. Once a NN has been trained, it can be assumed to be an "expert" in recognising the pattern or trend of the information it has been given to analyse. This feature of NN's can be used to provide projections for new situations of interest. NN's use a different technique of problem solving compared to conventional computers. Conventional computers follow instructions which are set out in order to solve a problem. This means that the steps that are supposed to be taken by the computer need to be known for the computer to solve a problem. Hence conventional computers can solve problems that are already understood and which can be solved. NN's on the other hand, learn the relationship between a given set of inputs and a known output in much the same way that the brain processes information [Stergiou and Siganos, 1996].

A large number of interconnections of neurons is used in NN's to achieve good performance. Neurons are nonlinear devices, hence NNs are nonlinear [Haykin, 1994]. A typical artificial neuron has many inputs and a few outputs and is often called a node, cell or unit. The nodes

receive inputs from other units or from external sources. The cells are connected to other cells by communication links each with its own weight. Each input has its own weight, w associated with it, which can be modified to model the learning. The information used by the net to solve the problem is represented by the weights [Fausett, 1994]. The nodes evaluate some function f of the weighted sum of the inputs (as shown in equation 4.1) and the output of the node can then serve as an input to other nodes. The computing power of NN's is derived from parallel distributed structure and the ability to learn. This enables NN's to produce reasonable outputs for inputs not met in the learning process. These features of the NN's enable them to solve complex problems that are currently impossible to solve [Haykin, 1994].

$$y_j = f\left(\sum_i w_{ij} x_i\right) \tag{4.1}$$

where the weighted sum $\sum_j w_{ij} x_i$ is called the net input to unit i or written as net_i and w_{ij} refers to the weight from unit j to unit i. x_i and y_j are the input and output to unit i respectively.

NN's offer a clear example of learning known as supervised learning where the connection weights are adjusted by inputting a set of training samples. The training samples are picked at random from the training set. Each input is unique and has its corresponding output. The network then calculates the errors and the weights are adjusted accordingly to minimize the difference between the actual output and the desired output. A large sample is used in the training, so that the network reaches a steady state where there are insignificant changes in the connection weights. After each iteration in the learning process the network becomes more knowledgeable about the task it is being trained for. The network learns by making a mapping of inputs to outputs from the given sample [Haykin, 1994].

There are two operational modes for a neuron: the training mode and the testing (using) mode. When in the training mode, the neuron can be taught to be on (fire or 1) or to be off (not to fire or 0) for particular input patterns. In the testing mode, when the inputs detect a taught pattern, their corresponding output becomes the current output. In case where the input pattern is not in the taught list of input patterns, a rule is used to determine whether to fire or not. The neuron will only be on (fire) if the input pattern is similar or close to some taught pattern. This is sometimes called the firing rule. An example of a simple artificial neuron is shown in figure 4.1 [Stergiou and Siganos, 1996].

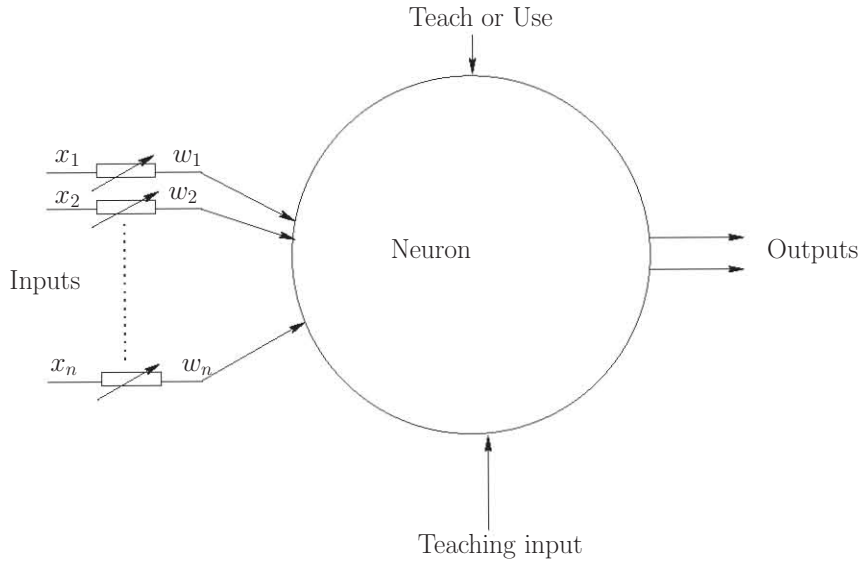

Figure 4.1: An example of a simple McCulloch Pitts (MCP) neuron. Adopted from Stergiou and Siganos, 1996.

An externally applied threshold θ_k or a bias term can also be included in NN models. Activation functions can be used in NN's to define the output of a neuron in terms of the activity level at its input. These will not be discussed in this thesis and information on them can be found in Haykin (1994).

Pattern recognition is an important application of the neural networks. A feed-forward neural network that has been trained accordingly can be used for pattern recognition. The network is trained to associate outputs with input patterns. The network identifies the input pattern and tries to give an output which is best associated with the input. When a pattern that has no output associated with it is given as an input, the NN provides the output that corresponds to a taught input pattern that differs least from the given pattern. The feed-forward NN's allow signals to travel in one direction only, hence the output of any layer does not affect the same layer because there is no feedback [Stergiou and Siganos, 1996]. To minimize the total squared errors of the output computed by the net, a training method known as backpropagation can be used. Note that signals are sent in the reverse direction during the backpropagation stage of learning [Fausett, 1994]. The backpropagation algorithm is discussed in the next section.

A more complicated neuron is the McCulloch and Pitts model (MCP), which has weighted inputs as explained earlier. The effect of the weighting is that each input makes a decision dependent on the weight of the input. The weight of an input is multiplied with the input to

give a weighted input, and the weighted inputs are then added. If the sum of the weighted inputs is greater than a pre-set value (v), the neuron will fire, otherwise the neuron will not fire. Thus the neuron fires if and only if [Stergiou and Siganos, 1996]:

$$x_1w_1 + x_2w_2 + x_3w_3 + ... + x_nw_n > v \tag{4.2}$$

The MCP has the advantage of adapting to particular situations by just changing its weights or the pre-set value. A number of algorithms that cause the neuron to adapt are available, but they will not be discussed here. The most popular ones are the delta rule and the back-propagation. The algorithm which is used in the modeling of the shape parameters will be discussed in the next section.

4.2.1 Architecture of neural networks

Network layers

The most common and simplest type of NN has three layers of nodes. These layers are connected together. A layer of input units is connected to a layer of hidden units, which is in turn connected to a layer of output units as shown in figure 4.2. This is an example of a feed-forward multi-layered neural network, with one layer of hidden units. The output cells and the hidden cells may also have biases as explained in Fausset (1994). There are also feedback networks, which have signals travelling in both directions. These will be not discussed in this thesis since the feed forward backpropagation network was used.

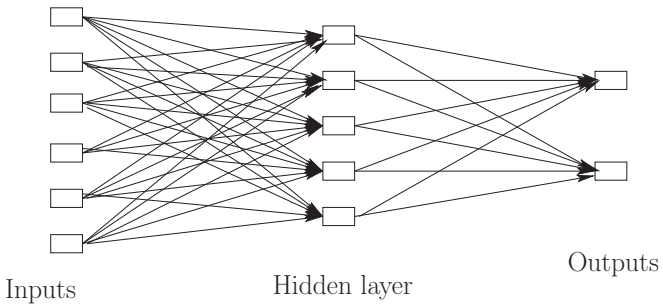

Figure 4.2: An example of a simple feed-forward network

The input units represent the raw information that is fed into the network. The hidden units are activated by the input units and the associated weights on the connections between the inputs and the hidden layers. The output units are activated by the hidden units together with their associated weights between the hidden layer and the output units. The

hidden units are allowed to construct their own representation of the inputs. The activation of each hidden unit is determined by the weights between the inputs and the hidden layer and by adjusting the weights, a hidden cell can choose what it represents. Single layer networks which have all the units connected to each other are the most general case and have more computational power than the multi-structured multi-layered networks [Stergiou and Siganos, 1996].

For a neural network to perform some task, it has to be trained and this entails adjusting the weights of each unit so that the difference between the desired output and the actual output is reduced. This process entails the computation of the error derivative of the weights (EW) by the NN's. The NN calculates how the error changes as each weight is increased or decreased slightly. The most extensively used algorithm for determining the EW is the backpropagation [Stergiou and Siganos, 1996].

It is easy to see how the backpropagation algorithm works if all the units are linear. An extra step is needed if the units in the network are non-linear as shown in equation (4.6) to equation(4.9). In this algorithm, the EA's are calculated first, then converted to EI's and eventually converted to EW's (where EA is the derivative of the error with respect to the activity of an output and EI is the derivative of the error with respect to the total input received by an output cell). In the case of output units, the EA is just the difference between the desired and the actual output. The computation of the EA is shown below [Stergiou and Siganos, 1996].

The weight associated with a connection is a real number and is known as the weight of the connection. This is denoted by w_{ij} and it is the weight associated with the connection between unit j and unit i. The pattern of connectivity in the network can thus be represented by a weight matrix W which has elements w_{ij}. There are two types of connections: excitatory and inhibitory. An excitatory connection is represented by a positive weight while the inhibitory connection is represented by a negative weight. A unit in the output layer will follow two steps to determine its activity. First, the total weight of the input y_j is computed using equation (4.3), then the activity x_j is computed using some function of the total weighted input. A sigmoid function can be used for this function as shown in equation (4.4) [Stergiou and Siganos, 1996]

$$y_j = \sum_i x_i w_{ij} \tag{4.3}$$

with x_i being the activity level of the j^{th} cell in the previous layer and w_{ij} the weight of the connection between the i^{th} node of the previous layer and the j^{th} node of the subsequent layer.

The activity x_j of a node is calculated using a function of the total weighted inputs known as the sigmond function, equation (4.4):

$$x_j = \frac{1}{(1 + e^{-y_j})} \tag{4.4}$$

The network will then compute the error E once the activities of all the output units have been determined using the following formula:

$$E = \frac{1}{2} \sum_i (x_i - d_i)^2 \tag{4.5}$$

Here x_i is the activity level of the i^{th} unit in the preceding layer and d_i is the output of the i^{th} unit. There are four steps associated with the backpropagation algorithm:
First compute EA using the following formula

$$EA_j = \frac{\partial E}{\partial x_j} = x_j - d_j. \tag{4.6}$$

Then EI is computed from the result of EA

$$EI_j = \frac{\partial E}{\partial y_j} = \frac{\partial E}{\partial x_j} \times \frac{dx_j}{dy_j} = EA_j x_j (1 - x_j). \tag{4.7}$$

Next, find EW by multiplying EI by the activity level of the unit from which the connection originates

$$EW_{ij} = \frac{\partial E}{\partial W_{ij}} = \frac{\partial E}{\partial y_j} \times \frac{\partial y_j}{\partial W_{ij}} = EI_j y_j. \tag{4.8}$$

Finally, the rate of change of the error as the activity of a unit in the previous layer is changed can be computed. Backpropagation can be applied to multilayer networks because of this step. The changing of the activity of a unit in the previous layer affects the activities of the output units it is connected to, hence all these effects on the outputs are added together to get the final error. This is achieved by multiplying EI by the weight on that connection, as shown below. This procedure can be repeated as many times as needed to get the EA's for all the previous layers in multi-layered networks.

$$EA_i = \frac{\partial E}{\partial x_i} = \sum_j \left(\frac{\partial E}{\partial y_j} \times \frac{\partial y_j}{\partial x_i} \right) = \sum_j EI_j W_{ij} \tag{4.9}$$

Backpropagation training of a network involves three stages:

1. Input training pattern feed-forward.
2. Calculation and backpropagation of the errors.
3. Adjustment of the weights.

A multi-layered feed-forward network is what is known as the backpropagation network. Input node signals are fed forward through the hidden layer processing units to the output cells. The comparison of the output and the desired results is then completed and the error is sent (propagated) backwards from the output layer through the hidden layers. The weights of each of the connections is then adjusted accordingly, hence the name "backpropagation" [Stergiou and Siganos, 1996].

Once the training has been completed, the net only uses the computations of the feed-forward phase. The algorithm used in this model is the feed-forward backpropagation.

4.2.2 The learning process

Pattern memorisation and the response of the network can be divided into two broad groups: associative mapping and regularity detection. For further reading on these, refer to Stergiou and Siganos (1996). The power of all NN's is contained in the values of the connection weights. The information in a net is stored in a weight matrix W and the learning process is the determination of the weights. There are two types of NN's:
1. Fixed networks, where the weights are fixed and cannot be changed, that is $\frac{dW}{dt} = 0$, and

2. Adaptive networks, where the weights are allowed to change, that is $\frac{dW}{dt} \neq 0$. [Stergiou and Siganos, 1996]

Adaptive networks can be subdivided into two main groups: supervised learning and unsupervised learning. For further information on these, refer to Stergiou and Siganos (1996). ANN's behaviour is dependent on the weights and the input-output function that is given to the nodes. In this model, the sigmoid function is used, but there are other functions which can be used, like the linear function. Sigmoid nodes resemble real neurons better than other types of nodes. Here the input changes as the output varies continuously, but not linearly.

During feed-forward an input signal x_i is received by each input unit X_i and this signal is relayed to each of the nodes, Z_j in the hidden layer. The activation is then computed by each of the hidden cells and the signal z_j sent to the output. The activation y_k of the output node Y_k is then computed to form the response of the net for the provided input pattern [Fausett, 1994].

During the learning process, output cells compare their computed activation y_k with the target value t_k to determine the error for the pattern for each node. The factor δ_k is then computed based on each error. The factor δ_k is used to correct the weights between the hidden layer and the output and to distribute the error to all the cells in the hidden layer. Another factor δ_j is computed for each hidden node Z_j for the correction of the weights between the inputs and the hidden nodes [Fausett, 1994]. The weights for all the layers will be adjusted after all the δ factors have been computed. Having a large hidden layer or too many hidden layers can degrade the quality of the network performance. More on the choice of the number of hidden layers and units can be found in Orr et al (1999).

4.3 Training the NN

A total of 11 years data was used for the NN model namely 1996 to 2006 Grahamstown ionosonde data. The 1996 to 2005 data was used in the training of the NN. The 2006 data was not used in the training but was reserved for testing. The 2000 data was used for both testing and training the model.

One hidden layer with ten nodes was used for this preliminary model. The network was trained for each parameter separately, hence there was one output for each parameter. The inputs to the network were the solar index, the magnetic index, the day number, and the time of the day. The day number and the time of the day were converted to sine and cosine by equations (4.10) to (4.13). This was done for each data point for all the years and to avoid numerical discontinuities at the end of year and midnight boundaries [Poole and Mckinnell, 2000].

$$DS = sin\left(2\Pi \times \frac{DN}{365.25}\right) \tag{4.10}$$

$$DC = cos\left(2\Pi \times \frac{DN}{365.25}\right) \tag{4.11}$$

$$HS = sin\left(2\Pi \times \frac{Hr}{24}\right) \tag{4.12}$$

$$HC = cos\left(2\Pi \times \frac{Hr}{24}\right) \tag{4.13}$$

Here DS is the day number sine, DC is the day number cosine, DN the day number, HS the hour of the day sine, HC the hour of the day cosine and Hr is the decimal hour of the day.

The magnetic index and solar index were extracted from the Hermanus Magnetic Observatory (HMO) archived data with the help of a FORTRAN programme. The data was randomly sorted to prevent biasing in any particular area. The data file was sorted in random order and then normalised. The NN's were trained following the procedure of the Stuttgart Neural Network Simulator (SNNS). The SNNS is a software simulator developed by the Institute for Parallel and Distributed High Performance Systems (IPVR) at the University of Stuttgart for NN's on Unix workstations [http://www-ra.informatik.uni-tuebingen.de/SNNS/announce.html].

After starting the SNNS it is important to specify the network achitecture. The number of inputs, hidden layers and outputs should also be selected at this point together with the number of nodes for each layer. The inputs were either five or six depending on the exclusion or inclusion of the magnetic index. For all the parameters there was just one output. 70% of the data was used for the training and 30% for the testing. One hidden layer with ten units was used for all the predictions. The two-month running mean of the daily sunspot number R_2, was used for the B_0 and B_1 prediction whilst the one month running mean of the daily sunspot number R_1 was used for the prediction of D_1. These were chosen because they have in the past been successfully used in the prediction of F_2 and F_1 profile parameters respectively. The a_k index was used for the magnetic index, with the A_8 index being used for all the parameters in this prediction. The a_k index is measured every three hours, hence A_8 is a one-day running mean of the three-hourly a_k indices [Williscroft and Poole, 1996]. For each training, the number of iterations (cycles) was chosen as a thousand. The learning parameter was always set to 0.1 for all the predictions. For the operating procedures of the SNNS, refer to the SNNS users manual [Zell et al, 1993].

The IRI values used in this thesis were obtained without updating the IRI electron den-

sity profile with the measured peak parameters as recommended in Bilitza (2000).

4.4 Comparison with IRI models

4.4.1 B_0 variation

In this section the diurnal variation of the B_0 parameter during the solstice and equinox months is compared with the IRI-2001 model and the preliminary NN model. The NN's were run four times for this procedure, with the magnetic index (R_1 or R_2) and the solar index (A_8) as input parameters and then with only the solar index (R_1 or R_2) as the input parameter. The root mean square errors were smallest when using the two-month running mean of the sunspot number R_2 as one of the inputs. The root mean square error (RMSE) is a measure of the difference between predicted values and the observed values. The formula for the calculation for the RMSE is given by equation (4.14). The presented graphs are those where only the solar index R_2 was used as an input parameter. In this section the particular days diurnal variation of the B_0 parameter was used instead of the monthly median representative data. Figure 4.3 shows the variations for the year 2000 whilst figure 4.4 shows the variations for the year 2006. Observed results are represented by red stars ($*$), the Gulyaeva's option is represented by black addition signs ($+$), the IRI-2001 tables method is represented by blue diamonds ($\blacklozenge$) and the NN prediction is represented by the green diamonds($\diamond$). It can be seen from the graphs that the NN prediction is more accurate than the two IRI-2001 options for the winter period during the daytime in both years. The year 2000 prediction is more accurate than the year 2006 prediction, partly because the year 2000 data was used in the training set. The RMSE for the different input parameters for the year 2006 are shown in table 4.1. The root mean square values shows that the NN prediction is more accurate than the IRI-2001 model when using R_2 as an input parameter. The NN model predicts B_0 values that are lower than the measured values (underpredicting the B_0 parameter) for all the seasons excluding winter at noon in 2006. One other interesting thing in the diurnal plots is that the daily variation is clearly evident just as much as in the monthly median plots.

$$RMSE = \sqrt{\frac{\sum_{i=1}^{n}(x_{1,i} - x_{2,i})^2}{n}} \tag{4.14}$$

Here $x_{1,i}$ and $x_{2,i}$ are the measured and the predicted values respectively.

!

Inputs	NNs	IRI tables	Gulyaeva
R_1	28.36 km	33.62 km	28.31 km
R_1A_8	32.95 km	33.62 km	28.31 km
R_2	23.58 km	33.62 km	28.31 km
R_2A_8	24.64 km	33.62 km	28.31 km

Table 4.1: The root mean square errors for 2006 B_0 shape parameter with the NN method using different combinations of the input parameters compared to the IRI-2001 tables method and the Gulyaeva option

A similar picture is found in the annual variation with the NN model being the more accurate model when compared to both the IRI-2001 tables method and the Gulyaeva option (figure 4.5). The NN model performs better when predicting the daytime annual variation as compared to the nighttime annual variation. In the mid-night annual variation all three options predict B_0 values that are higher than the measured values (overpredicting the B_0 parameter). The NN model overpredicts the noon annual variation for the winter in the year 2006 but does well for the summer, autumn and spring periods. The 2000 NN model predicts well for all the seasons.

4.4.2 B_1 variation

In this section the preliminary NN model is compared to the daily observed data and the IRI-2001 model for the solstice and equinox months. Only the year 2006 predictions were determined using the NN model. Figure 4.6 shows the diurnal variation of the B_1 parameter together with the NN preliminary model and the IRI-2001 tables model. Observed results are represented by red stars ($*$), the IRI-2001 tables method is represented by blue diamonds ($\blacklozenge$), whilst the NN prediction is represented by green diamonds($\diamond$). The root mean square values are presented in table 4.2 and have been calculated using equation (4.14). The two-month running mean of the daily sunspot number R_2 was used for this prediction since it provided the least root mean square error when predicting for B_0. From the root mean square error it can be seen that the NN model predictions are more accurate than the IRI-2001 model. The prediction with the solar index and the magnetic index as input parameters give a slightly larger root mean square error value as compared to the prediction using the solar index only (i.e. without the use of the magnetic index). The NN was able to pick up the sudden increase of the parameter at around 03h00 to 04h00 UT and around 20h00 UT.

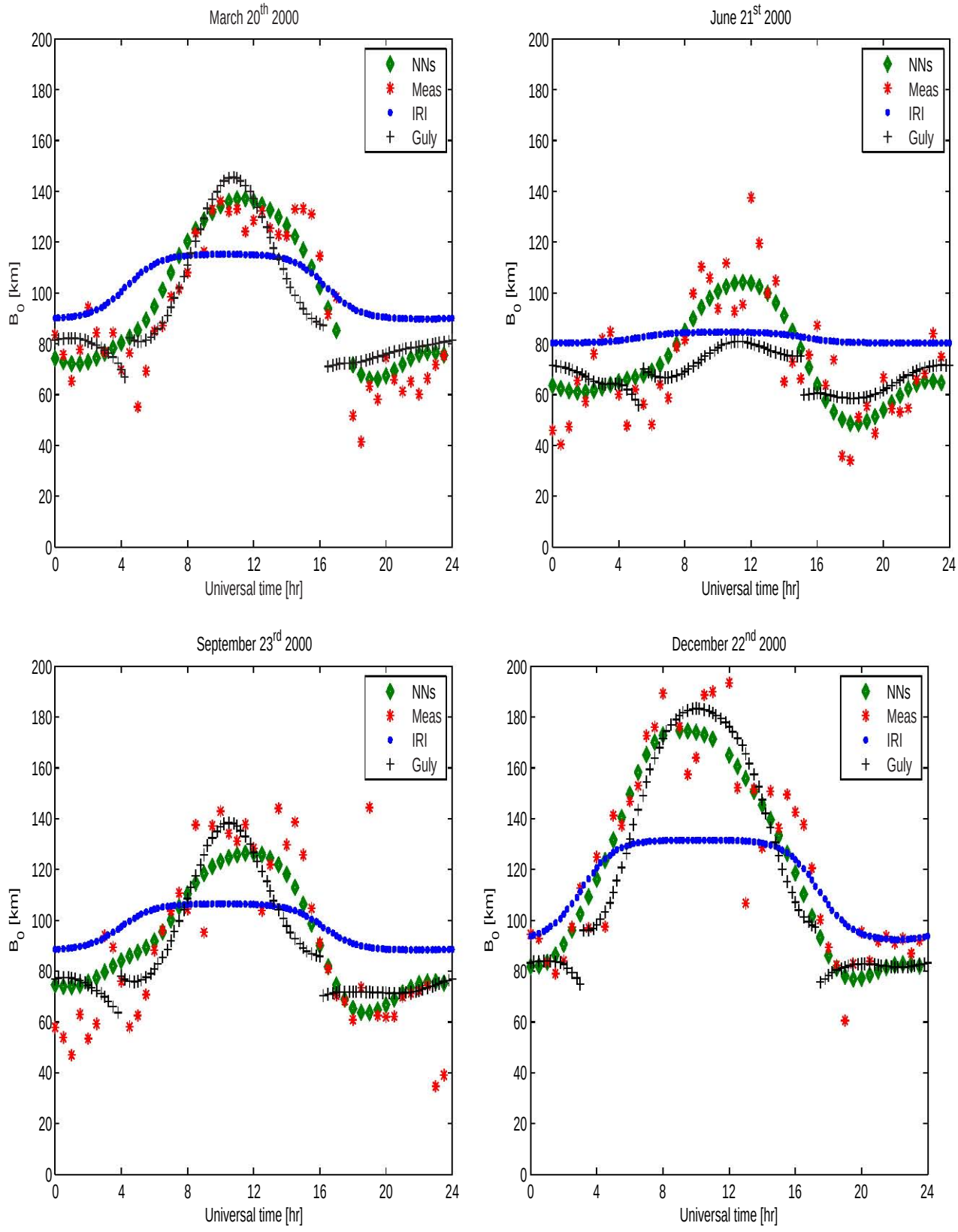

Figure 4.3: Comparison of the diurnal variations of the B_0 parameter over Grahamstown during 2000 using the IRI-2001 model, the Gulyaeva option and the NN preliminary model.

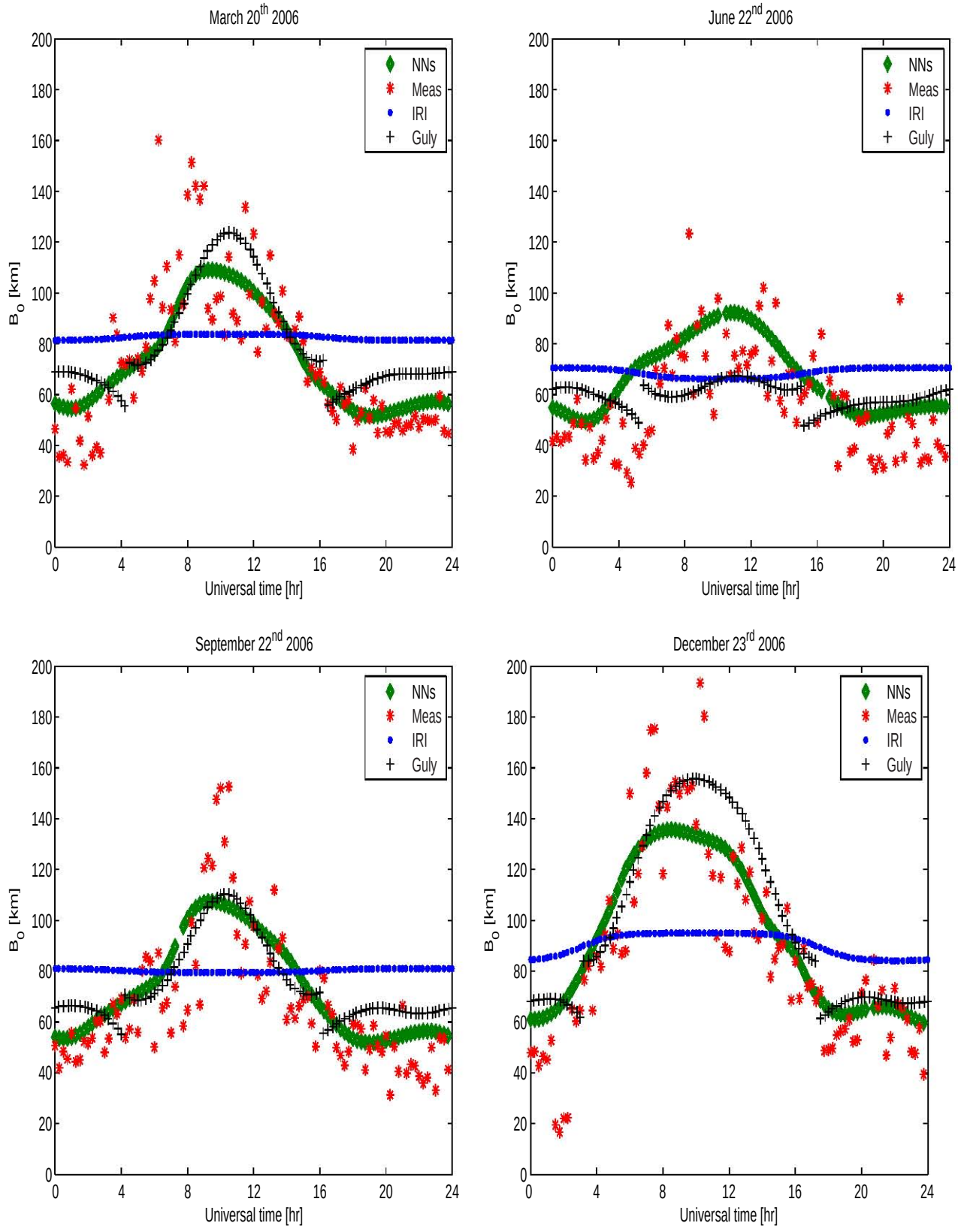

Figure 4.4: Comparison of the diurnal variations of the B_0 parameter over Grahamstown during 2006 using the IRI-2001 model, the Gulyaeva option and the NN preliminary model.

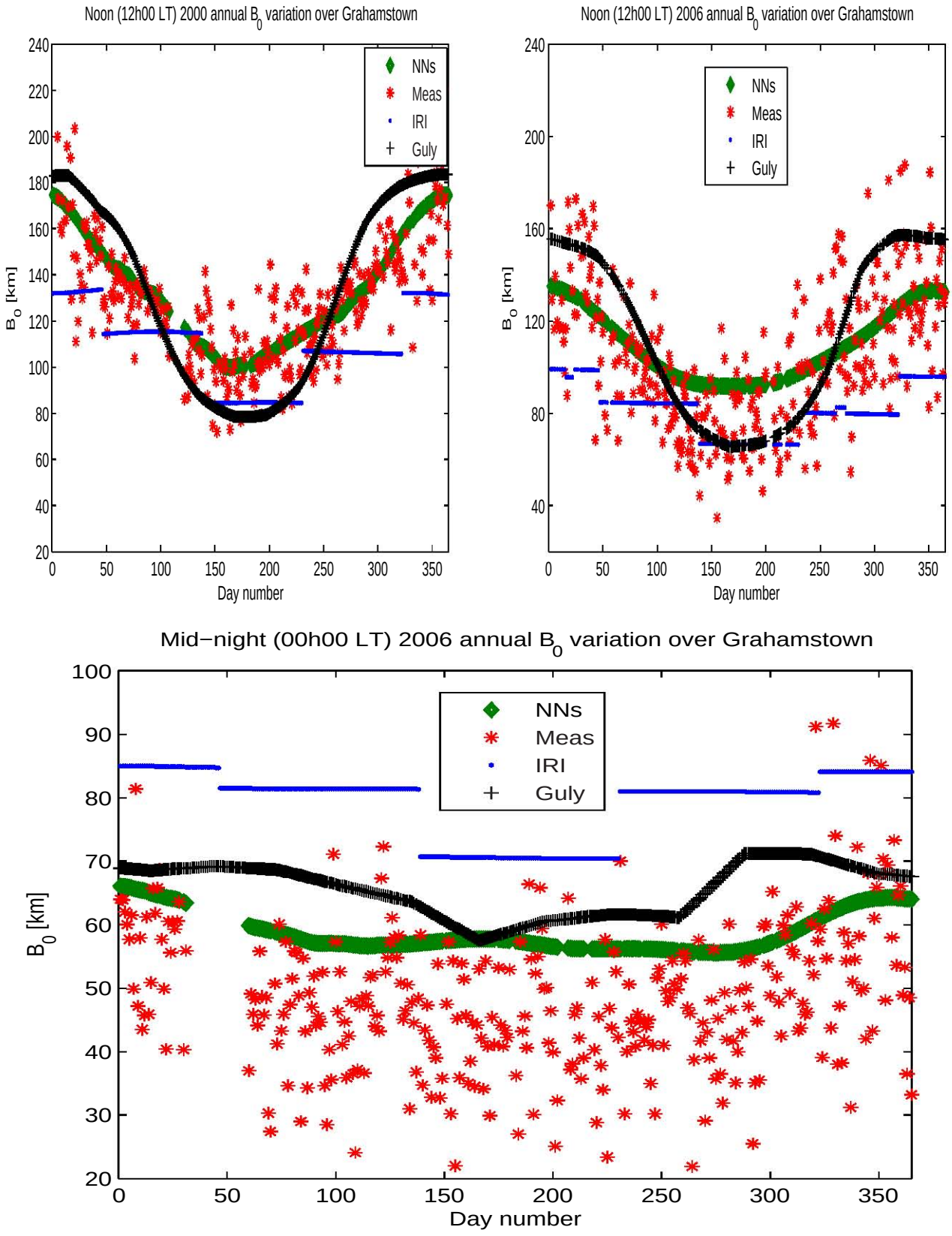

Figure 4.5: Comparisons of the annual B_0 variations over Grahamstown using the IRI-2001 model, the Gulyaeva option and the preliminary NN model.

Inputs	NNs	IRI tables
R_2	0.401	0.428
R_2A_8	0.406	0.428

Table 4.2: The root mean square errors for 2006 B_1 shape parameter with the NN method using different combinations of the input parameters, compared to the IRI-2001 tables method.

The local noon annual variation of B_1 shows larger values of B_1 in the winter which is reflected in the NN predictions (figure 4.7). The IRI model shows no variations for both the local noon and local mid-night B_1 variation. The local mid-night B_1 variation is inconclusive, due large variations in the measured B_1 parameter. The measured B_1 parameter values did not reveal any conclusive annual variation pattern. It is unclear at this time if this is a true reflection of the ionospheric behaviour of this parameter, or if an inherent problem exists within the data. Currently in the IRI B_1 is set to 3 and increased in increments of 0.5 if merging between the F_2 bottomside profile and the E-valley can not be accomplished [Bilitza et al, 2000]. This might be the source of the problems in the extraction of B_1 since a significant number of the data points are below the IRI set value of 3. If the determination and extraction of B_1 by ARTIST is not good, this could affect the NN model since the model uses the measured data in the training of the model.

4.4.3 D_1 variation

In this section the observed diurnal variation of the D_1 parameter in the solstice and equinox months is compared with the IRI-2001 model and the preliminary NN model. The NN was trained four times for this procedure, with the magnetic index (A_8) and the solar indices (R_2 or R_1) as input parameters and twice with only the solar indices as the input parameter. The root mean square errors are smallest for the prediction with the one-month running mean of the daily sunspot number R_1. The presented graphs are therefore those where R_1 was used as an input but not the magnetic index. Table 4.3 shows the root mean square error values calculated from equation (4.14) for each training of the NN's. In this section the diurnal variation of the D_1 parameter for a particular day was used instead of the monthly median representative data. Figure 4.8 shows the D_1 variations for the year 2006. Observed results are represented by red stars ($*$), the IRI-2001 tables method is represented by blue diamonds ($\blacklozenge$), whilst the NN prediction is represented by green diamonds($\diamond$). It can be seen from the graphs and the root mean square error values that the NN prediction is more accurate at predicting D_1 than the IRI-2001 tables method for all the seasons.

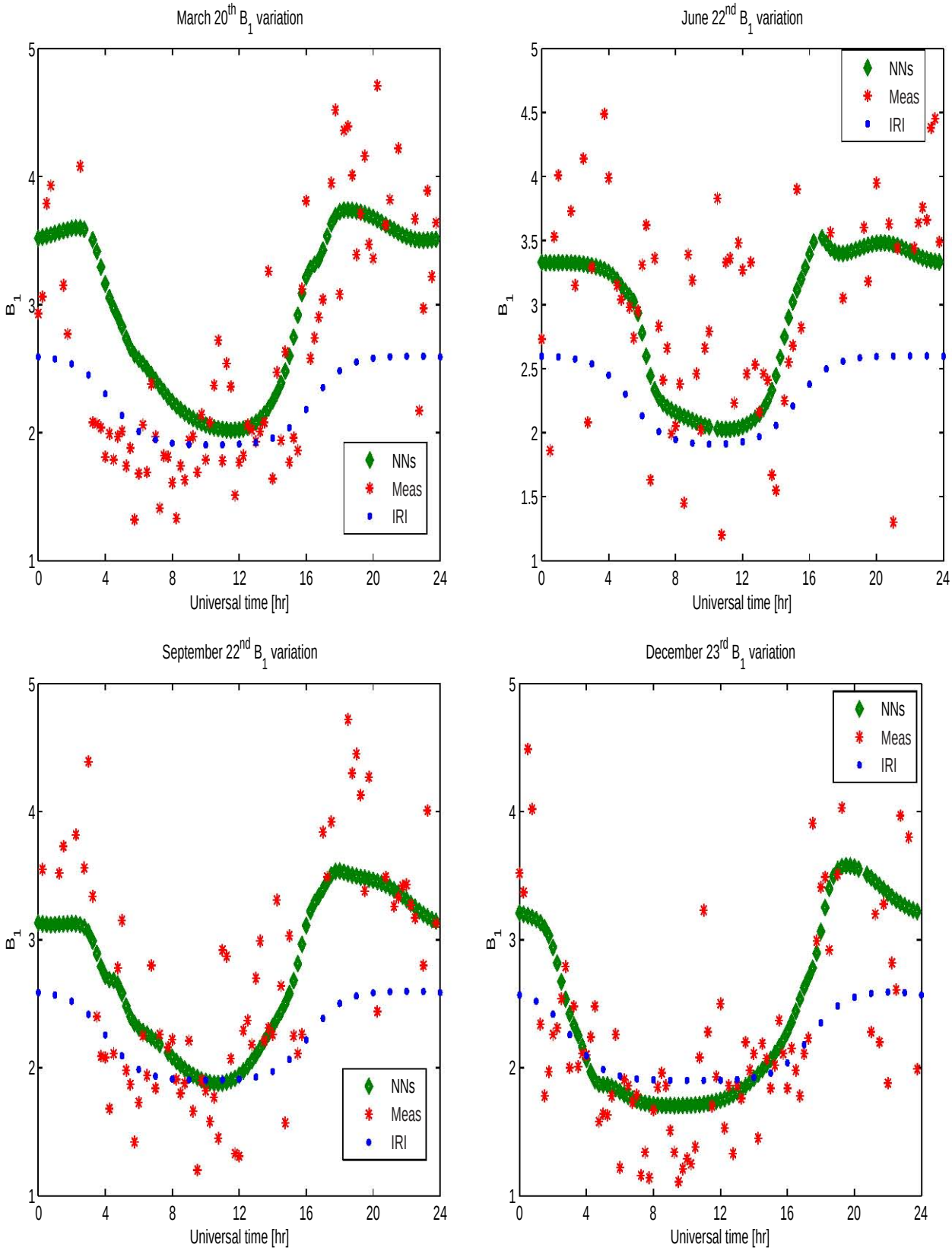

Figure 4.6: Comparison of the diurnal variations of the B_1 parameter over Grahamstown during 2006 using the IRI-2001 model and the NN preliminary model.

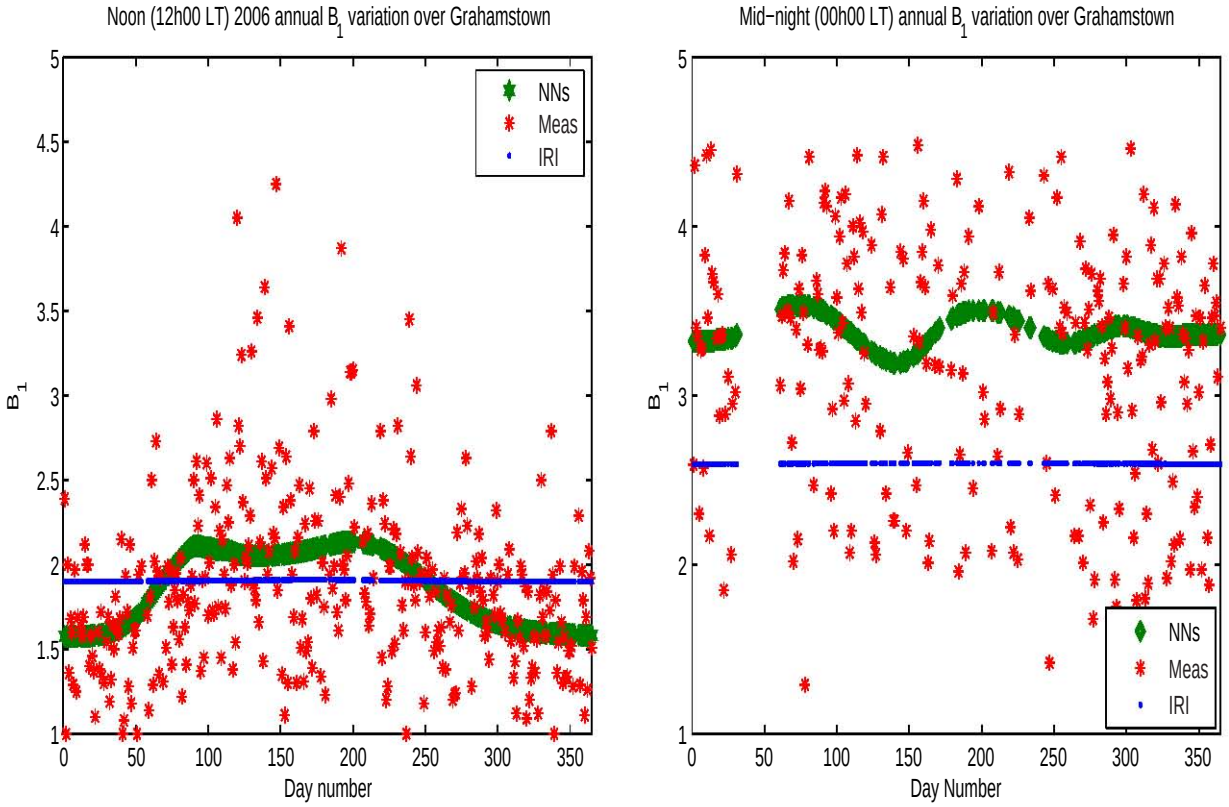

Figure 4.7: Comparisons of the annual B_1 variations over Grahamstown using the IRI-2001 model and the preliminary NN model.

Inputs	NNs	IRI tables
R_1	0.254	0.350
R_1A_8	0.261	0.350
R_2	0.257	0.350
R_2A_8	0.262	0.350

Table 4.3: The root mean square errors for 2006 D_1 shape parameter with the NN method using different combinations of the input parameters, compared to the IRI-2001 tables method.

The annual variations of the D_1 parameter are inconclusive since most of the data points are set at either 0.5 or 1 (figure 4.9). This could be a problem with the extraction of the parameter by ARTIST since it has been seen that there can be difficulties in the characterisation of the F_1 layer by ARTIST due to degraded ray tracing performance [Jacobs et al, 2004]. The formula (equation 2.13) for the F_1 layer makes the F_1 layer peak height very dependent on the half thickness of the F_2 layer. Hence finding a better F_1 layer description is dependent on having a good description of the F_2 region [Reinisch and Huang, 1999]. This means that if there are errors in the description of the F_2 region, they will affect the value of D_1. The IRI profile given by equation (2.13) is not a good representation of the F_1 layer at low latitudes as discovered by Reinisch and Huang (1996). This could still be the problem for this mid-latitude station which will affect the values of the extracted D_1. Results by Jacobs et al (2004) showed that there are possible shortcomings in the ability of ARTIST to characterise the F_1 layer due to poor scaling. It has been seen that at times raytracing performance is degraded due to difficulties in the real-time characterisation of the F_1 layer by ARTIST. This could be another reason for the poor quality of the D_1 data collected at Grahamstown. The NN's preliminary model could still pick up the annual variation, with the minimum D_1 found in winter and the maximum D_1 found in the equinox months (March and September). The results show that the IRI-2001 tables method underpredicts the parameter. The root mean square error for the NN's model is smaller compared to the error when using the IRI-2001 tables method.

4.5 Conclusion

The results in this chapter show that there may be errors in the extraction of both B_1 and D_1 parameters by the ARTIST scaling program. The formulae describing their respective regions could also be not adequate in describing the profiles. Generally, the NN models for the three parameters provide more accurate results compared to the IRI-2001 model. The NN model could still pick up some variation in the annual variation of the D_1 parameter even though the data is "unreliable". This should be investigated further.

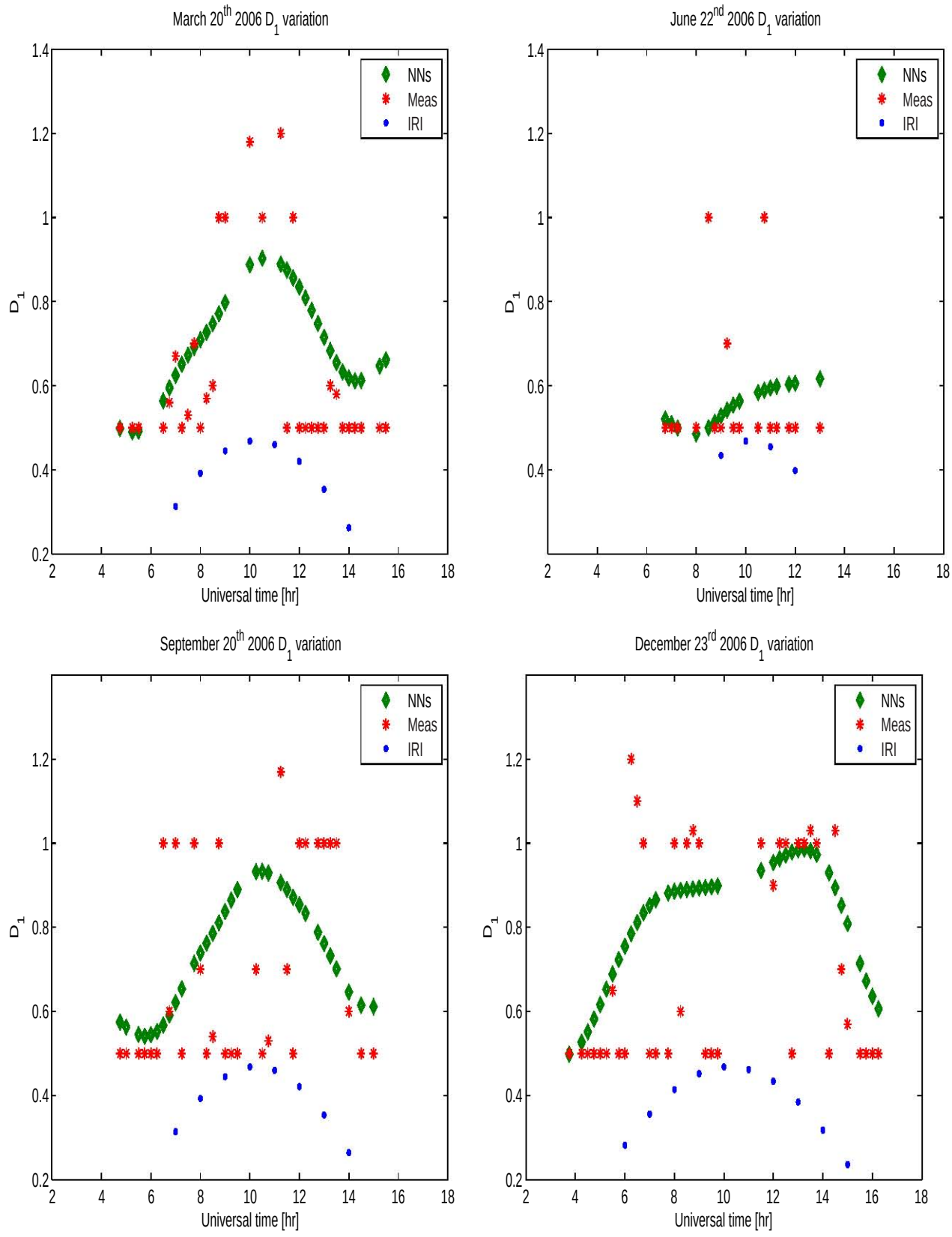

Figure 4.8: Comparison of the diurnal variations of the D_1 parameter over Grahamstown during 2006 using the IRI-2001 model and the NN preliminary model.

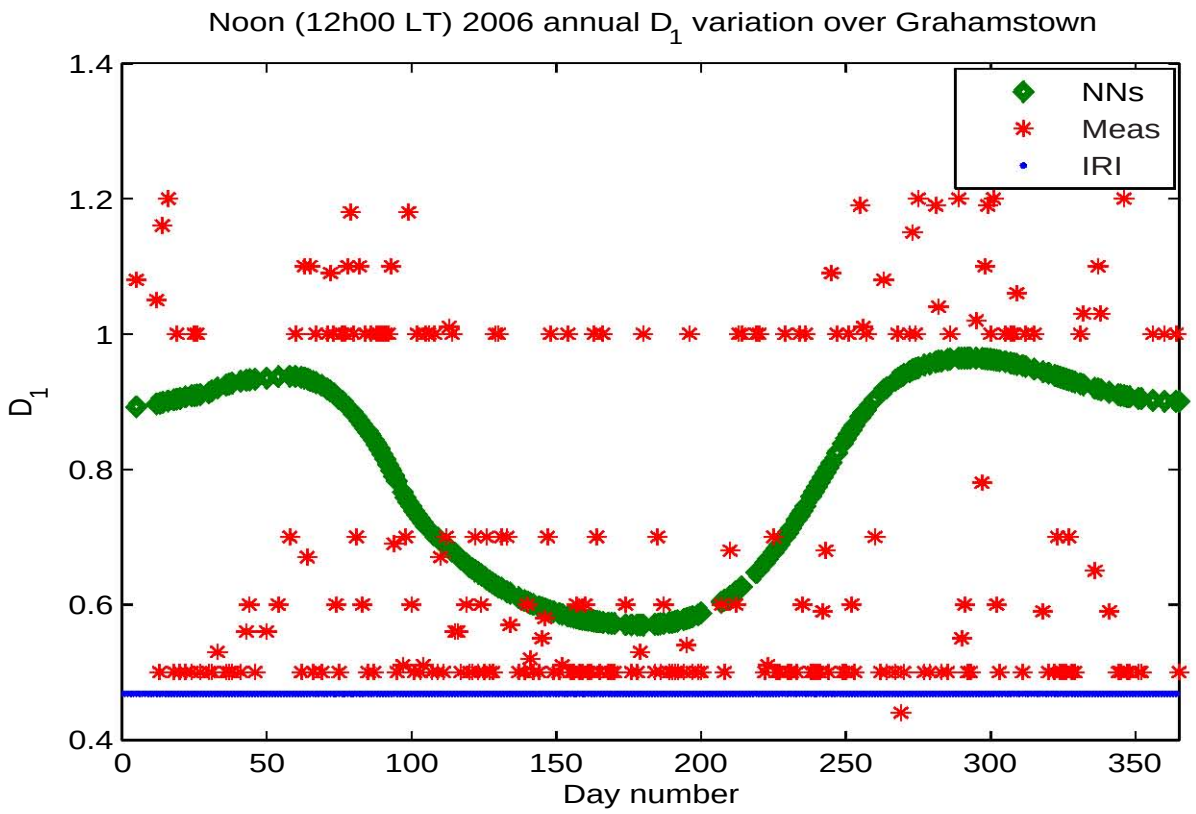

Figure 4.9: Comparisons of the annual D_1 variations over Grahamstown using the IRI-2001 model and the preliminary NN model.

Chapter 5

Discussion and conclusions

5.1 Discussions and recommendations

The investigation of the variation of the IRI shape parameters, B_0, B_1 and D_1 over Grahamstown, South Africa was carried out using archived Grahamstown data. Three preliminary models were then developed using NN's for each parameter and compared to the IRI-2001 model. This chapter offers the discussion and recommendations for further research in this area.

The IRI tables method assumes constant daytime values for B_0 which is clearly not the case as seen from the plots based on values extracted from ionosonde measurements. There is a clear peak around local noon for all the seasons. The IRI assumes that B_0 is minimum during the daytime in winter, which is not the case as observed from the winter diurnal B_0 plots. The IRI-model can be improved to have a smooth diurnal variation of B_0 until a peak at local noon. Other local or global models can also be developed to help in the prediction of the shape parameters. There is a need to interpolate the IRI-2001 tables option for the annual prediction so that the variation is smooth with a minimum in the winter. Epstein functions can be used in the model for the annual prediction to get a smooth transition from season to season. From the plots it can be seen that the annual nighttime variation is small (about 40 km) compared to the daytime annual variation (about 130 km). In general, the observed seasonal B_0 variations at midnight are different from those predicted by the IRI-2001 model. The results of the bottomside thickness parameter given by the Gulyaeva option are generally in better agreement with the observed ionosonde data. It has been observed that the Gulyaeva option predicts B_0 reasonably for summer (December) and spring (September) compared to predictions for the other seasons. The diurnal variation of B_0 shows greater values during the day reaching the maximum at around 10h00 UT. This is because during

the day there is greater production rate and small loss, but at night the production rate is smaller and the loss is greater. The production rate is related to the zenith angle as follows: the smaller the zenith angle the higher the production rate. Hence there is a peak in the B_0 observed graphs at around 10h00 UT which is around local noon. The production rate as a function of height is also affected by the density which increases downwards and the intensity of the radiation which decreases downwards.

From the plot of the noon B_1 annual variation it can be seen that the measured values of B_1 are mostly below 3, but in the IRI B_1 is set to 3 and then increased in increments of 0.5 if merging between the F_2 bottomside profile and the E-valley cannot be accomplished. This could lead to problems for the daytime merging of the profiles of the two regions. Based on the measured data the best choice of B_1 for this area would be 1.5 or 2 during the day and about 3 for the nighttime. Further investigation should be undertaken into the variability of the parmeters, not only with time, but also with location around the subcontinent. The diurnal variation of B_1 shows greater values during the night, reaching the maximum at around 02h00 UT and 18h00 UT. The prediction of B_1 by the IRI tables method is better for the nighttime than the daytime especially for the equinox months and the winter time. The IRI model overpredicts the shape parameter B_1 in summer and under predicts the parameter for all the other seasons.

The annual variation plots for D_1 suggest that there may be a problem in the extraction of the parameter. This could be due to the incorrect scaling by ARTIST as explained in Jacobs *et al* (2004), the definition of the IRI F_1 layer by equation (2.13) as explained in Reinisch and Huang (1999) or the determination of the probability of the F_1 presence as explained in Radicella *et al* (1998). The way in which ARTIST-4 automatically extracts and calculates the parameter may be improved. The formulae describing the F_1 region can also be improved upon for better observed values of D_1. The diurnal variation plots for B_1 suggest that the IRI-2001 tables method should be improved to predict the parameter more accurately, especially during the nighttime. More work needs to be done in order to get a better understanding of the annual variation of both D_1 and B_1 since the annual variation plots are inconclusive. The problem with the extracted D_1 parameter can be clearly seen in the plots for D_1. The NN model produces a prediction of the D_1 parameter with the parameter minimum in winter and maximum in the equinox months. This should be studied further to determine whether the NN prediction is a true representation of the actual variable. An investigation of the function of the F_1 layer could be undertaken to improve the F_1 layer representation and this could lead to improved predictions of the parameter.

The IRI tables method should be improved or replaced to provide more accurate predic-

tions of these parameters.

The predictions by the NN-based model could be improved by training NNs for different combinations of solar indices and magnetic indices and obtaining an optimum input space. The number of iterations could also be varied to improve the model.

5.2 Conclusions

This thesis presented an investigation into the variability and predictability of the IRI shape parameters over Grahamstown, South Africa. The major conclusions emerging from this investigation are:-

1. The bottomside thickness parameter B_0 is always maximum at around local noon, the shape parameter B_1 is always minimum at around local noon and the shape parameter D_1 is always maximum at around local noon.

2. The shape parameter of the F_1 layer is present for a small time during the winter as compared to other seasons and its value is also small for the wintertime. The parameter is only observed for 4 hours some days in the winter from around 08h00 UT to about 12h00 UT. During the autumn and spring it can be observed from about 06h00 UT to 14h00 UT. Finally, in the summer it can be observed from about 04h00 UT to about 16h00 UT.

3. The investigation shows the need to improve the extraction of the D_1 parameter and/or improve the formula describing the F_1 region. The need for improving the IRI F_1 profile has been discussed by Reinisch and Huang (1999) and could be a factor in the inconclusive results of the D_1 parameter. An investigation into the actual problem around the D_1 results could be done to pinpoint the source of the problem.

4. The IRI B_0 annual prediction needs to be updated and interpolated to give a smooth annual variation.

5. The investigation shows that there is a need to update the IRI model with the Grahamstown results, because of the discrepancies between the IRI tables method and the observed results.

6. The preliminary NN model has proven to be the more accurate method for the prediction of the IRI shape parameters and future work will include developing this technique

further.

7. There is a need to do more work on the NN's to improve their prediction by investigating more combinations of input parameters and different numbers of nodes in the hidden layer. An investigation into the effect of altering the number of iterations on the error could also be done. Doing a similar study for other parts of South Africa and the subcontinent could lead to the updating of the IRI model and help in the fomulation of other models.

The objective of this study, namely to investigate the suitability of the IRI-2001 model to predict the IRI shape parameters and to develop a more accurate alternative model for the prediction of the parameters for Grahamstown has been accomplished. This project has shown that a predictive model for the IRI shape parameters can be developed, however, significant research is required into improving the parameters derived from measurements if an accurate model is required. Results from this study are of interest to the IRI community in the quest to constantly improve the global ionospheric predictions.

References

- Bilitza D., *International Reference Ionosphere*, 1990, NSSDC/WDC-A-R&S 90-22, Science Applications Research, USA
- Bilitza D., Radicella S. M., Reinish B. W., Adeniyi J. O., Mosert Gonzalez M. E., Zhang S. R., Obrou O., *New B_0 and B_1 models for IRI*, 2000, Advances in Space Research, Vol 22, pp 89-95
- Bilitza D, *International Reference Ionosphere* 2000, 2001, Radio Science, Vol 36, pp 261-275
- Davies K., *Ionospheric Radio*, 1990, Vol. 31 of IEE Electromagnetic Waves Series, Peter Peregrinus, London, ISBN 086341186X
- Davis C., *Basic Ionosonde theory*, 1998, The Ionospheric monitoring group, Rutherford Appleton Laboratory *http : //www.wdc.rl.ac.uk/ionosondes/ionosonde_basics. html*
- Ducharme E. D., Petrie L. E., Eyfrig R., *A Method for Predicting the F_1 layer Critical Frequency*, 1971, Radio Science, Vol 6, pp 369-378
- Ducharme E. D., Petrie L. E., Eyfrig R., *A Method for Predicting the F_1 layer Critical Frequency Based on Zurich Smoothed Sunspot number*, 1973, Radio Science, Vol 8, pp 837-839
- Fausett S., *Fundamentals of Neural Networks*; *Architectures*, *Algorithms and Applications*, 1994, Prentice Hall, Inc., New Jersey 07632 USA
- Gulyaeva T.L., *Progress in ionospheric informatics based on electron density profile analysis of ionogram*, 1987, Advances in Space Research, Vol 7, PP 39-48
- Haykin S., *Neural Networks*, *A Comprehensive Foundation*, 1994, Macmillan College Publishing Company

- Jacobs L, Poole A. W. V., McKinnell L. A., *An Analysis of Automatically Scaled F_1 Layer Data over Grahamstown, South Africa*, 2004, Advances in Space Research, Vol 34, pp 1949-1952

- Kohl H., Rüster R., Schlegel K., *Modern Ionospheric Science*, 1996, European Geophysical Society

- Langley R. B. *GPS, the Ionosphere, and the Solar Maximum*, 2000, GPS World pp 44-49 *http* : *//gauss.gge.unb.ca/papers.pdf/gpsworld.july*00*.pdf*

- Lee Chien-Chih, Reinish B.W, *Quiet − condition h_mF_2, N_mF_2, and B_0 variations at Jicamarca and comparison with IRI* − 2001 *during solar maximum*, 2006, Journal of Atmospheric and Solar-Terrestrial Physics, Vol 68(18), pp 2138-2146

- Olazábal B. L., Cuartas K. A, Rodríguez González M., Calzadilla Méndez A., *Diurnal variations of B_0 parameters over Havana at low solar activity*, 2004, Geofísica Internacional, Vol 43, pp 125-128

- Orr G, Schraudolph N., Cummins F., *Neural Networks*, Lecture notes, 1999, Willamette University, *http* : *//www.willamette.edu/* ∼ *gorr/classes/cs*449*/intro.html*

- Poole A. W. V., McKinnell L, *On the Predictability of foF_2 Using Neural Networks*, 2000, Radio Science, vol 35, pp 225-234

- Radicella S. M., Bilitza D., Reinisch B. W., Adeniyi J. O., Mosert González M. E., Zolesi B., Zhang M. L., Zhang S. R., *IRI task Force Activity at ICTP*: *Proposed Improvements for the IRI Region Below the F Peak*, 1998, Advances in Space Research, Vol 22(6) pp 731-739

- Ramakrishnan S., Rawer K., *Model Electron Contnet Density Profiles Obtained by Empirical Procedures*, 1972, Space Research XII, 1253-1259

- Rawer K., Bilitza D., Ramakrishnan S., *Goals and Status of the International Reference Ionosphere*, 1978, Rev. Geophysics. 16, pp 177-181,

- Rawer K. *Joint Analytical profile of Electron Density Profiles with Epstein Functions*, 1987, Advances in Space Research Vol. 7(6) pp 25-33

- Reinisch B. W., Huang X., *Low latitude Digisonde Measurements and Comparison with IRI*, 1996, Advances in Space Research, Vol. 18, pp 5-12

- Reinisch B. W., Xueqin Huang, *Finding Better B_0 and B_1 Parameters for the IRI F_2 Profile Function*, 1998, Advances in Space Research Vol. 22, pp 741-747

- Reinisch B. W., Huang X., *Redefining the IRI F_1 Layer Profile*, 2000, Advances in Space Research, Vol. 25, pp 81-88
- Reinisch B. W., Galkin I., Sales G. S., Bullet T. W., *Real Time Ionospheric Characteristics from the Digisonde Network for Data Assimilation Systems*, 2003, European Geophysical Society, Vol. 5 07258
- Rishbeth H., Mendillo M., *Patterns of $F_2 - layer\ variability$*, 2001, Journal of Atmospheric and Solar-Terrestrial Physics, Vol. 63(2001) pp 1661-1680
- SAO-Explorer User's Guide, University of Lowell Massachusetts, Center for Atmospheric research, Interactive Ionogram Scaling Technologies, *http* : *//ulcar.uml.edu/ARTIST*4*/Offline.html*, retrieved November 2006
- Sethi N. K., Pandey V. K., *Comparative Study of Electron Density from Incoherent Scatter Measurements at Arecibo with the IRI*$-$95 *Model during Solar Maximum*, 2001, Annales Geophysicae 18, pp 1630-1634
- South African Ionospheric Data Center, *http* : *//ionosond.ru.ac.za*, retrieved September 2006
- SNNS, Institute for parallel and distributed high performance systems, University of Stuttgart *http* : */www* $-$ *ra.informatik.unituebingen.de/SNNS/announce.html*, retrieved August 2007
- Stergiou C., Siganos D., *Neural Networks*, 1996, *http* : *//www.doc.ic.ac.uk/* $\sim$ *nd/surprise_*96*/journal/vol*4*/cs*11*/report.html*
- UMLCAR, Reprocessing Digisonde data with ARTIST-4 software, University of Lowell Massachusetts, Center for Atmospheric research, Interactive Ionogram Scaling Technologies, *http* : *//ulcar.uml.edu/ARTIST*4*/Offline.html*, retrieved November 2006
- Williscroft L., Poole A.W. V., *Neural Networks*, foF_2, *Sunspot Number and Magnetic Activity*, 1996, Geophysical Research letters, vol 23, pp 3659-3662
- Zhang M. L., Shi J. K., Liu L., *Variation Behaviour of the Bottomside B_0 and B_1 Parameters Obtained from the Ground*$-$*Based Ionograms at China's low Latitude Station*, Advances in Space Research, In press, 2007
- Zell A., Mache N., Hübner R, Günter Mamier, Vogt M., Herrmann K., Schmalzl M., Sommer T., Hatzigeorgiou A., Döring S., Posselt D., *SNNS* : *Stuttgart Neural Network Simulator*, 1993, Institute for Parallel and Distributed High Performance Systems, University of Stuutgart, Fed. Rep. of Germany, *http* : *//citeseer.ist.psu.edu/zell*93*snns.html*